Ground-State Equilibrium Thermodynamics and Switching Kinetics of Bistable [2]Rotaxanes Switched in Solution, Polymer Gels, and Molecular Electronic Devices

ARTICLE *in* CHEMISTRY · JANUARY 2006

Impact Factor: 5.73 · DOI: 10.1002/chem.200500934 · Source: PubMed

DOI: 10.1002/chem.200500934

Ground-State Equilibrium Thermodynamics and Switching Kinetics of Bistable [2]Rotaxanes Switched in Solution, Polymer Gels, and Molecular Electronic Devices

Jang Wook Choi,[a] Amar H. Flood,[b, d] David W. Steuerman,[a, e] Sune Nygaard,[c] Adam B. Braunschweig,[b] Nicolle N. P. Moonen,[b] Bo W. Laursen,[b, f] Yi Luo,[a] Erica DeIonno,[a] Andrea J. Peters,[b] Jan O. Jeppesen,*[c] Ke Xu,[a] J. Fraser Stoddart,*[b] and James R. Heath*[a]

Abstract: We report on the kinetics and ground-state thermodynamics associated with electrochemically driven molecular mechanical switching of three bistable [2]rotaxanes in acetonitrile solution, polymer electrolyte gels, and molecular-switch tunnel junctions (MSTJs). For all rotaxanes a π-electron-deficient cyclobis(paraquat-*p*-phenylene) ($CBPQT^{4+}$) ring component encircles one of two recognition sites within a dumbbell component. Two rotaxanes ($RATTF^{4+}$ and $RTTF^{4+}$) contain tetrathiafulvalene (TTF) and 1,5-dioxynaphthalene (DNP) recognition units, but different hydrophilic stoppers. For these rotaxanes, the $CBPQT^{4+}$ ring encircles predominantly (>90%) the TTF unit at equilibrium, and this equilibrium is relatively temperature independent. In the third rotaxane ($RBPTTF^{4+}$), the TTF unit is replaced by a π-extended analogue (a bispyrrolotetrathiafulvalene (BPTTF) unit), and the $CBPQT^{4+}$ ring encircles almost equally both recognition sites at equilibrium. This equilibrium exhibits strong temperature dependence. These thermodynamic differences were rationalized by reference to binding constants obtained by isothermal titration calorimetry for the complexation of model guests by the $CBPQT^{4+}$ host in acetonitrile. For all bistable rotaxanes, oxidation of the TTF (BPTTF) unit is accompanied by movement of the $CBPQT^{4+}$ ring to the DNP site. Reduction back to TTF^0 ($BPTTF^0$) is followed by relaxation to the equilibrium distribution of translational isomers. The relaxation kinetics are strongly environmentally dependent, yet consistent with a single electromechanical-switching mechanism in acetonitrile, polymer electrolyte gels, and MSTJs. The ground-state equilibrium properties of all three bistable [2]rotaxanes were reflective of molecular structure in all environments. These results provide direct evidence for the control by molecular structure of the electronic properties exhibited by the MSTJs.

Keywords: calorimetry · kinetics · molecular devices · rotaxanes · thermodynamics

[a] J. W. Choi, Dr. D. W. Steuerman, Dr. Y. Luo, E. DeIonno, K. Xu, Prof. J. R. Heath
Division of Chemistry and Chemical Engineering (127–72)
California Institute of Technology, 1200 E. California Blvd.
Pasadena, CA, 91125 (USA)
Fax: (+1) 626-395-2355
E-mail: heath@caltech.edu

[b] Dr. A. H. Flood, A. B. Braunschweig, Dr. N. N. P. Moonen, Dr. B. W. Laursen, Dr. A. J. Peters, Prof. J. F. Stoddart
California NanoSystems Institute and
Department of Chemistry and Biochemistry
University of California, Los Angeles, 405 Hilgard Avenue
Los Angeles, CA, 90095-1569 (USA)
Fax: (+1) 310-206-1843
E-mail: stoddart@chem.ucla.edu

[c] S. Nygaard, Prof. J. O. Jeppesen
Department of Chemistry
Odense University (University of Southern Denmark)
Campusvej 55, 5230, Odense M (Denmark)
Fax: (+45) 66-15-87-80
E-mail: joj@chem.sdu.dk

[d] Dr. A. H. Flood
Current Address: Department of Chemistry, Indiana University
800 East Kirkwood Avenue, Bloomington, IN 47405 (USA)

[e] Dr. D. W. Steuerman
Current Address: Department of Physics
University of California, Santa Barbara CA 93106 (USA)

[f] Dr. B. W. Laursen
Current Address: Nano-Science Center
University of Copenhagen, Universitetsparken 5
2100, København Ø (Denmark)

Introduction

One of the goals[1–3] of the field of molecular electronics is to be able to control the properties of molecular-based solid-state devices through chemical design and synthesis. Such control has been demonstrated[4–9] for passive devices, the simplest of which are molecular tunnel junction resistors consisting of a molecular monolayer, often a functionalized alkane, sandwiched between two conductors. Several groups have shown that the tunnel current varies exponentially with chain length,[6] although they have also found that atomistic details,[7–8] such as the packing of the chains, the molecular alignment within the monolayer, and the nature of the electrodes,[9] are all important.

Molecular rectifiers, typically represented by an electron-donor–bridge–acceptor molecule extended between two electrodes,[10] represent a more sophisticated passive device. Demonstrations of molecular control over current rectification have required a substantial effort by a number of groups,[10–18] and have only been achieved within the past few years. Details such as the nature of the molecule/electrode interface, the donor and acceptor molecular orbital energies, and the structure of the molecule within the device—that is, the extension of the donor–bridge–acceptor between the two electrodes—are all important, since rectification can arise from many areas within a junction.[10–18]

Active molecular electronic[19] devices (switches) represent a significant jump in terms of molecular complexity. We have reported previously[20–22] on the use of electrochemically switchable, donor–acceptor, bistable [2]catenane and [2]rotaxane molecular-switch tunnel junctions (MSTJs). As in the case of the molecular tunnel junction resistors and rectifiers, MSTJs also represent a highly coupled molecule/electrode system.[9,23–24] However, for the bistable [2]catenane and [2]rotaxane switches, there are a number of experimental parameters that can be measured to correlate molecular structure and solution-phase switching behavior with molecular electronic-device-switching properties. These parameters include colorimetric changes,[25] shifts in electrochemical potentials,[26–27] and temperature-dependent kinetics[25–27] for the cycling of the switch.

As an example, consider the redox-switchable [2]rotaxane $RATTF^{4+}$ illustrated in Figure 1a. This bistable [2]rotaxane is composed of π-electron-accepting cyclobis(paraquat-*p*-phenylene) ($CBPQT^{4+}$) ring (blue) that encircles either a tetrathiafulvalene (TTF) unit (green) or a 1,5-dioxynaphthalene (DNP) unit (red), both π-electron-donating systems. This mechanically interlocked molecular compound and other closely related bistable rotaxanes,[28] as well as rotaxanes constructed from different donor–acceptor units[29] or from hydrogen-bonded systems[30] and transition-metal templates,[31] have been investigated in depth previously. Under ambient conditions in acetonitrile, the $CBPQT^{4+}$ ring in $RATTF^{4+}$ encircles the TTF unit preferentially (>90%) with respect to the DNP unit. This equilibrium is described by the ΔG_{298} change shown in Figure 1b, in which $\Delta G = +1.6\ kcal\,mol^{-1}$ when the $CBPQT^{4+}$ ring moves from the

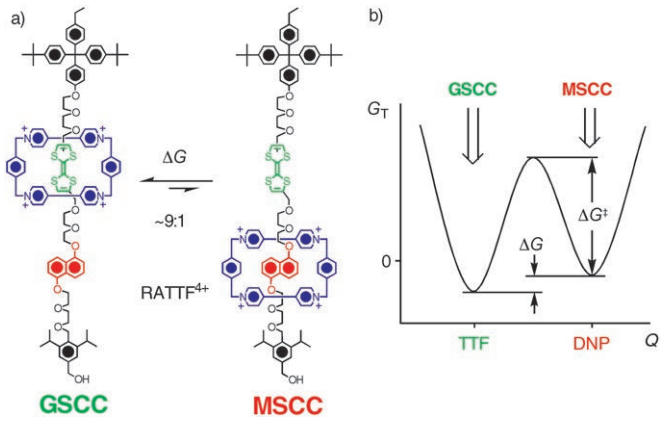

Figure 1. a) Structural formulas of the two translational isomers of the bistable rotaxane $RATTF^{4+}$ corresponding to the ground-state co-conformation (GSCC) and the metastable-state co-conformation (MSCC). b) Potential-energy surface for the bistable $RATTF^{4+}$, in which the energy wells correspond to the GSCC and MSCC. The free-energy difference ΔG, between the wells and the free-energy barrier to relaxation, $\Delta G^{\ddagger}$, from the MSCC to the GSCC are defined against a normal coordinate, Q, representing translation of the ring along the dumbbell component of the [2]rotaxane.

TTF to the DNP unit. Hence, the co-conformation (CC) with the $CBPQT^{4+}$ ring encircling the TTF unit is referred to as the ground-state co-conformation (GSCC). The first two oxidation states of $RATTF^{4+}$ correspond to the $TTF^0 \rightarrow TTF^{\cdot+} \rightarrow TTF^{2+}$ processes. Upon formation of $TTF^{\cdot+}$ radical cation, Coulombic repulsion between the $CBPQT^{4+}$ ring and the $TTF^{\cdot+}$ results[25–28] in the translation of the ring to the DNP unit. This process[32] is fast and is believed to convert all of the GSCC into the MSCC. When the $TTF^{\cdot+}$ radical cation is reduced back to TTF^0, the $CBPQT^{4+}$ ring remains around the DNP unit for a period of time. This translational isomer of the GSCC is the metastable-state co-conformation (MSCC). Recovery of the MSCC/GSCC equilibrium distribution (~1:9) is an activated process. This switching cycle can be detected by a number of experimental observations. First, the lowest oxidation potential (corresponding to $TTF^0 \rightarrow TTF^{\cdot+}$) of the GSCC is +490 mV, while that for the MSCC is +310 mV. (All potentials referenced to an Ag/AgCl electrode.) Second, the colors of GSCC- and MSCC-dominated solutions are green and red, respectively. Thus, electrochemistry and spectroscopy can be employed to quantify the MSCC/GSCC ratio in such a bistable rotaxane at any given time. Third, the (activated) relaxation of an MSCC- back to a GSCC-dominated distribution is temperature dependent, and so the kinetic parameters may be quantified through time- and temperature-dependent measurements. For example, the $\Delta G^{\ddagger}_{298}$ for this process in the case[27] of $RATTF^{4+}$ in the solution phase is 16.2(±0.3) kcal mol^{-1}.

We have recently reported on the MSCC→GSCC relaxation kinetics for a number of bistable [2]catenanes and [2]rotaxanes in several different environments, including 1) in acetonitrile,[27] 2) in monolayers ([2]rotaxanes only) bonded to the surfaces of Au working electrodes,[26] and 3) in solid-state polymer electrolytes.[25] In the case of the ace-

tonitrile and the polymer electrolyte devices, we have demonstrated[25,27] that the relaxation kinetics were sensitive to both molecular structure and physical environment, although the overall switching mechanism remains the same. In this paper, we extend these measurements to include MSTJ devices, as well as establishing the ground-state equilibrium thermodynamics. Three bistable [2]rotaxanes—namely RATTF^{4+}, RTTF^{4+}, and RBPTTF^{4+}—plus the control[33] [2]rotaxane RBLOCK^{4+} were investigated. It is evident from inspection of the structural formulas of these three [2]rotaxanes shown in Figures 1 and 2 that RATTF^{4+}, RTTF^{4+} and RBPTTF^{4+} can exist at equilibrium as two translational isomers (or co-conformations). By contrast, RBLOCK^{4+} has the CBPQT^{4+} ring located exclusively around the DNP unit as a result of the presence of the bulky SEt group on the monopyrrolotetrathiafulvalene unit, acting as an effective steric barrier, and thus preventing translational isomerism. The critical difference in the molecular structures between the RATTF^{4+} and RTTF^{4+} pair and the RBPTTF^{4+} lies with the replacement of the simple TTF unit for the bispyrrolotetrathiafulvalene (BPTTF) unit.[34] However, all three bistable rotaxanes have slightly different stoppers—RATTF^{4+} bears a substituted benzylic alcohol function and both RTTF^{4+} and RBPTTF^{4+} have slightly different hydrophilic stoppers facilitating their incorporation into MSTJ devices. The major difference in the switching properties between these bistable rotaxanes is that the equilibrium MSCC/GSCC ratio (~1:9) for RATTF^{4+} and RTTF^{4+} is relatively temperature independent, while the equilibrium MSCC/GSCC ratio (~1:4 at 298 K) for RBPTTF^{4+} exhibits a strong temperature dependence. These thermodynamic differences will be rationalized in this paper by reference to binding constants obtained by isothermal titration calorimetry (ITC) for the complexation of model guests containing TTF, BPTTF, and DNP units, by the CBPQT^{4+} host in acetonitrile at 298 K.

Previously we have hypothesized[20–22,24,25,35] that the GSCC corresponds to the low-conductance (switch-open) state of an MSTJ, while the MSCC corresponds to the high-conductance (switch-closed) state. This hypothesis is consistent with many observations, including the shift in the oxidation potential of the TTF group that correlates with the switching from the GSCC to the MSCC structure. In addition, Goddard's group[36] has found by computational methods that the MSCC structure has extended electron delocalization—and thus enhanced conductivity—in comparison with the GSCC.

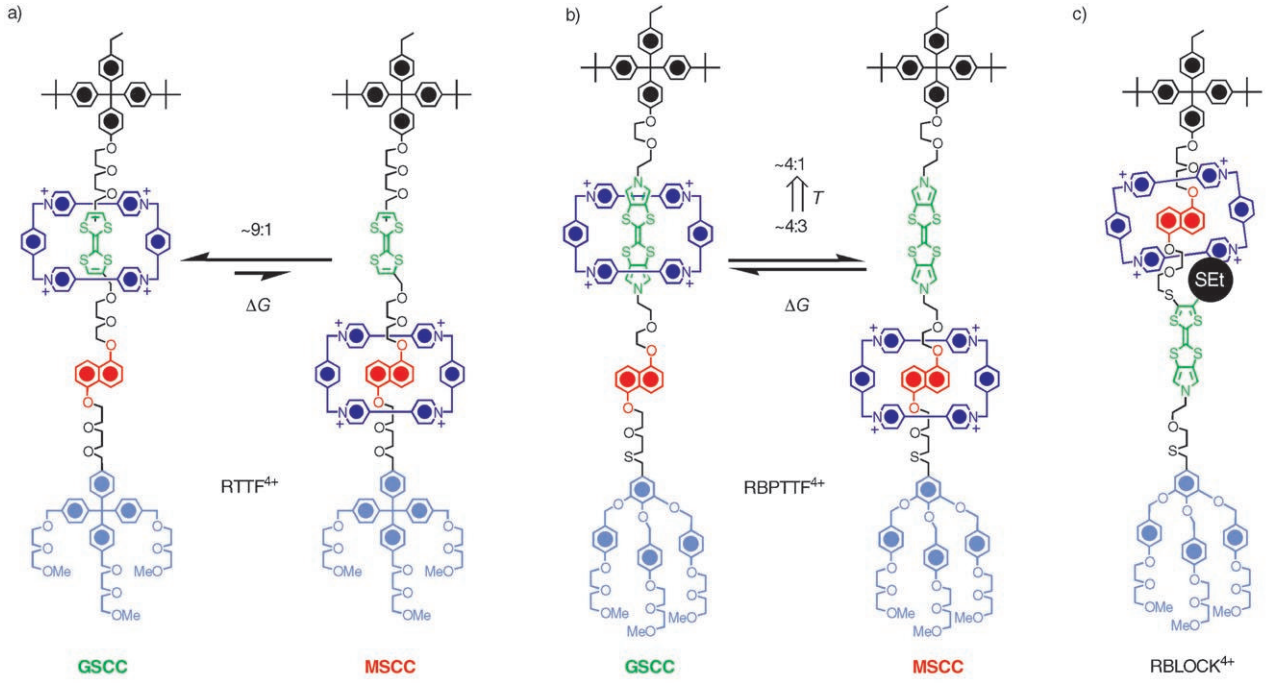

Figure 2. Structural formulas of the translational isomers of the bistable rotaxanes a) RTTF^{4+} and b) RBPTTF^{4+} both in their GSCC and MSCC. c) Structural formula of the sterically-blocked (SEt) [2]rotaxane RBLOCK^{4+} used in control studies.

The switching kinetics of RATTF^{4+}, RTTF^{4+}, and RBPTTF^{4+} should be relatively similar. By contrast, the ground-state thermodynamics—and hence the temperature dependence of the switching amplitude—should be quite different. In this paper, we employ temperature dependent electrochemical and current-voltage measurements to correlate *qualitatively* the thermodynamic properties of RATTF^{4+} in 1) acetonitrile and 2) solid-state polymer electrolytes, and of RTTF^{4+} in MSTJs together with RBPTTF^{4+} across all three environments. We also correlate *quantitatively* the MSCC→GSCC relaxation kinetics in these three different physical environments. We find that the ground-state thermodynamic differences between the pair of TTF-containing rotaxanes (RATTF^{4+} and RTTF^{4+}) and RBPTTF^{4+} are relatively independent of physical environment, but strongly

influenced by molecular structure. We also find that although the MSCC→GSCC relaxation kinetics exhibit a strong environmental dependence in the case of all three rotaxanes, the switching mechanism appears to be similar for all three compounds and is robust and consistent in all three environments. These findings allow us to refine our initial hypothesis such that the high-conductance (switch-closed) state of an MSTJ still corresponds to the MSCC, but that the low-conductance (switch-open) state is now related to the MSCC/GSCC ratio at equilibrium. These experiments provide a proof-of-principle for the control of molecular structure over a key device characteristic—temperature-dependent switching amplitudes in molecular electronic devices.

Results and Discussion

Molecular design: Although the bistable [2]rotaxanes $RATTF^{4+}$, $RTTF^{4+}$, and $RBPTTF^{4+}$ all contain DNP sites, they differ in that the first two contain a TTF unit and the third a BPTTF. To understand how these units influence the switching in these bistable rotaxanes, a series of model guests were investigated for their binding with the $CBPQT^{4+}$ host, as its tetrakis(hexafluorophosphate) salt, by using ITC. The model guests are shown in Figure 3a. They are tetrathiafulvalene (TTF) and its bispyrrolo derivative H_2BPTTF; their diethyleneglycol-disubstituted derivatives TTF-DEG and BPTTF-DEG; and 1,5-dioxynaphthalene (DNP-OH) and its diethyleneglycol-disubstituted derivative DNP-DEG. Addition of the DEG substituents to the TTF and DNP units is known[37] to enhance their binding constants with the $CBPQT^{4+}$ host to the extent that they increase by up to two orders of magnitude. By contrast, the binding of BPTTF by the $CBPQT^{4+}$ host is already quite high and only doubles.

The enthalpic contribution ΔH to the binding affinity K_a between DNP-DEG and the $CBPQT^{4+}$ host is similar (Table 1) to that for TTF-DEG, but it is almost double that for BPTTF-DEG. This larger difference between the enthalpy changes ΔH of association for the two complexes is also represented in the bistable rotaxanes by the enthalpy change ΔH of equilibrium associated with the affinity of the $CBPQT^{4+}$ ring

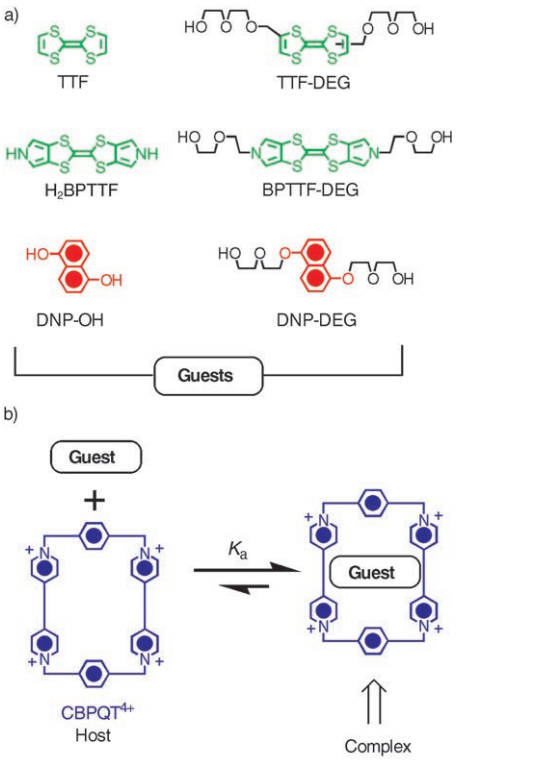

Figure 3. a) Structural formulas for a series of model guests. b) Host–guest complexation between the $CBPQT^{4+}$ host and each of the guests.

Table 1. Thermodynamic binding data[a] corresponding to the complexation between $CBPQT^{4+}$ and the individual components of the bistable rotaxanes in MeCN determined by isothermal titration microcalorimetry at 298 K[38] in addition to solution-phase thermodynamic data of bistable rotaxanes.

Guest	ΔH[b] [kcal mol^{-1}]	ΔS[c] [cal mol^{-1} K^{-1}]	ΔG[d] [kcal mol^{-1}]	K_a[c] [$\times 10^3$ M^{-1}]
TTF[e]	−10.64 ± 0.12	−18.1	−5.27 ± 0.03	6.9 ± 0.18
TTF-DEG	−14.21 ± 0.06	−22.1	−7.66 ± 0.07	380.0 ± 22.0
H_2BPTTF[f]	−9.00 ± 0.02	−7.9	−6.66 ± 0.03	70.8 ± 0.98
BPTTF-DEG	−8.20 ± 1.70	−3.6	−7.17 ± 0.12	168.0 ± 17.0
DNP-OH[g]	−16.04 ± 8.11	−41.7	−3.63 ± 0.36	0.44 ± 0.13
DNP-DEG[h]	−15.41 ± 0.02	−30.8	−6.26 ± 0.04	36.4 ± 0.25
$RATTF^{4+}$[i]	−2.82 ± 1.79[j]	−14.7 ± 6.8[j]	+1.56 ± 0.24	
$RBPTTF^{4+}$[i]	−6.64 ± 0.67	−26.0 ± 2.5	+1.11 ± 0.07	

[a] A 0.39 mM standard solution of $CBPQT^{4+}$ was used for all titrations into which solutions of various concentrations of guest were added in 5 μL aliquots (4.7 mM TTF; 3.2 mM TTF-DEG; 5.0 mM H_2BPTTF; 2.1 mM BPTTF-DEG; 5.4 mM DNP-OH; 3.9 mM DNP-DEG). [b] Under the constant pressure of the instrument, ΔH is obtained from the heat of the reaction.[38] [c] Fits were performed using software provided by Microcal LLC software, and the stoichiometry of all complexes was between 0.97 and 1.03 indicating a 1:1 complex was formed. [d] Calculated from the fitted value of K_a. [e] The binding constant for the complex formed between TTF and $CBPQT^{4+}$, previously measured in MeCN by the ^{1}H NMR single-point method, was determined to be 8000 M^{-1},[39a] and was found to be 10000 M^{-1} by the UV/Vis dilution method.[39b] [f] The binding constant for the complex formed between H_2BPTTF and $CBPQT^{4+}$, previously measured in Me_2CO by the UV/Vis dilution method, was determined to be 12000 M^{-1}.[40] [g] The binding constant for the complex formed between DNP-OH and $CBPQT^{4+}$, previously measured in MeCN by the UV/Vis dilution method, was determined to be 990 M^{-1}.[41] [h] The binding constant for the complex formed between DNP-DEG and $CBPQT^{4+}$, previously measured in MeCN by the UV/Vis dilution method, was determined to be 25400 M^{-1}.[41] [i] The given thermodynamic values for $RATTF^{4+}$ and $RBPTTF^{4+}$ were obtained by the variable temperature CV measurements, and they correspond to thermodynamic differences between the MSCC and GSCC; that is, the changes in H, S, and G when the $CBPQT^{4+}$ ring moves from the TTF(BPTTF) unit to the DNP unit. [j] The linear fit to $\Delta G/T$ vs $1/T$ for $RATTF^{4+}$ produced a low R^2 of 0.4 because the ΔG for $RATTF^{4+}$ was reasonably insensitive to temperature changes and therefore the data obtained reflects the standard error from the CV measurements.

for the two recognition units. Correspondingly, the bistable rotaxane RBPTTF^{4+} (−7.2 to −6.6 kcal mol^{-1} for association and equilibrium, respectively) shows a much higher ΔH than RATTF^{4+} (−1.2 to −2.8 kcal mol^{-1}, respectively). The direct consequence of this large ΔH difference of association between the complexes of the CBPQT^{4+} host with DNP-DEG and BPTTF-DEG guests is that the MSCC/GSCC ratio for RBPTTF^{4+} exhibits a strong temperature dependence, such that the ratio changes from 0.73 at 262 K to 0.25 at 284 K.[42] Moreover, this variable ratio should be detectable in all three environments. In the solution phase and polymer gels, the MSCC/GSCC ratio can be quantified directly through CV measurements. In the MSTJs, the temperature-dependent MSCC/GSCC ratio should be reflected in a temperature-dependent switching amplitude. By contrast with RBPTTF^{4+}, the smaller ΔH difference for the binding of the CBPQT^{4+} ring to the TTF and DNP units should favor a relatively temperature-independent MSCC/GSCC ratio in RATTF^{4+}, with the GSCC remaining the dominant co-conformation at all temperatures and in all environments, a situation that is indeed observed. Irrespective of these differences in the ground-state thermodynamics, for both RATTF^{4+} and RBPTTF^{4+} the actual electrochemically driven switching mechanism should be the same.

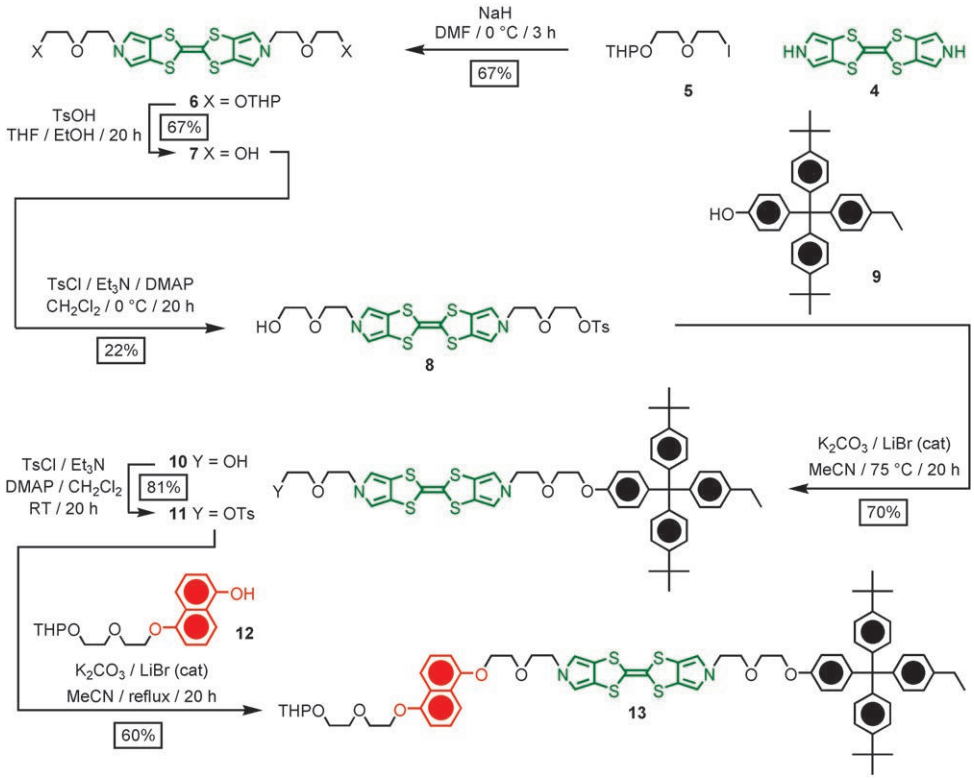

Scheme 1. Synthesis of the semi-dumbbell compound **13**.

Synthesis and characterization: The synthesis of the bistable rotaxanes RATTF^{4+} (Figure 1) and RTTF^{4+} (Figure 2) have been described elsewhere.[25,28d] UV-visible and ^{1}H NMR spectroscopy indicate that both these bistable rotaxanes exist predominantly (at least 90%) in the GSCC.

Synthesis of amphiphilic [2]rotaxane RBPTTF·4PF$_6$: The [2]rotaxane RBPTTF·4PF$_6$ was synthesized from precursors **1**–**3** according to the routes outlined sequentially in Schemes 1–3. Alkylation of H_2BPTTF[43] (**4**) with 2-[2-(2-iodoethoxy)ethoxy]tetrahydropyran[44] (**5**) in DMF gave the BPTTF derivative **6** in 67% yield (Scheme 1). Removal of the THP-protecting groups with *p*-toluenesulfonic acid (TsOH) gave the diol **7** in 67% yield. The monotosylate **8** was obtained in 22% yield by reaction of the diol **7** with one equivalent of *p*-toluenesulfonyl chloride (TsCl). Alkylation of the hydrophobic tetraarylmethane-based stopper[21] **9** with **8** in MeCN in the presence of K_2CO_3 gave the alcohol **10** (70%), which was tosylated by using TsCl in CH_2Cl_2 affording **11** in 81% yield. Subsequently, **11** was treated with the DNP derivative[28d] **12** under alkylation conditions (K_2CO_3/LiBr/MeCN) affording the BPTTF derivative **13** in 60% yield, which on treatment with TsOH in THF/EtOH, gave (Scheme 2) the alcohol **14** in 56% yield. The free hydroxyl function in compound **14** was thereafter converted to a tosylate group in 98% yield (**14**→**15**) and then to a thiocyanate group in 97% yield (**15**→**16**). The thiocyanate group was reduced in situ with $NaBH_4$, and the resulting thiolate was subsequently coupled with the hydrophilic chloride[21] **17** in THF/EtOH to give the dumbbell **1** in 68% yield. Finally, the [2]rotaxane RBPTTF·4PF$_6$ was self-assembled (Scheme 3) under high-pressure conditions by using the dumbbell compound **1** as the template for the formation of the encircling CBPQT^{4+} tetracation; the [2]rotaxane RBPTTF·4PF$_6$ was isolated in 47% yield from a mixture of the dumbbell compound **1**, the dicationic precursor[45] **2**·2PF$_6$, and the dibromide **3** after they had been subjected to a 10 kbar pressure in DMF at room temperature for three days.

RBPTTF^{4+} exists as a mixture of the two possible isomers in which the CBPQT^{4+} ring is located around the BPTTF unit in the GSCC and around the DNP unit in the MSCC. These two isomers give rise to characteristic charge-transfer (CT) absorption bands centered on 825 (GSCC) and 550 nm (MSCC), respectively, in the electronic absorption spectrum. The equilibrium population ratio can be determined from

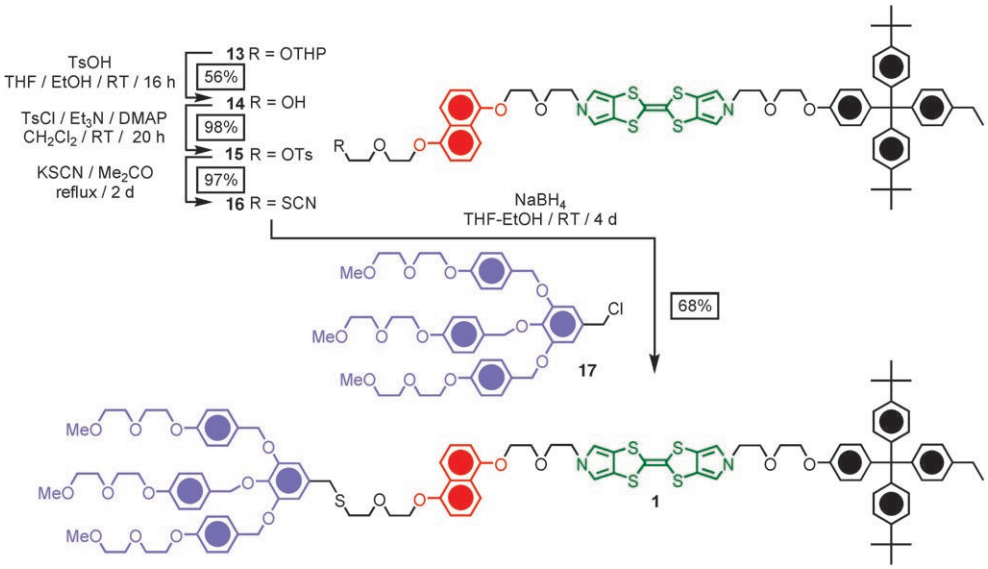

Scheme 2. Synthesis of the dumbbell compound **1**.

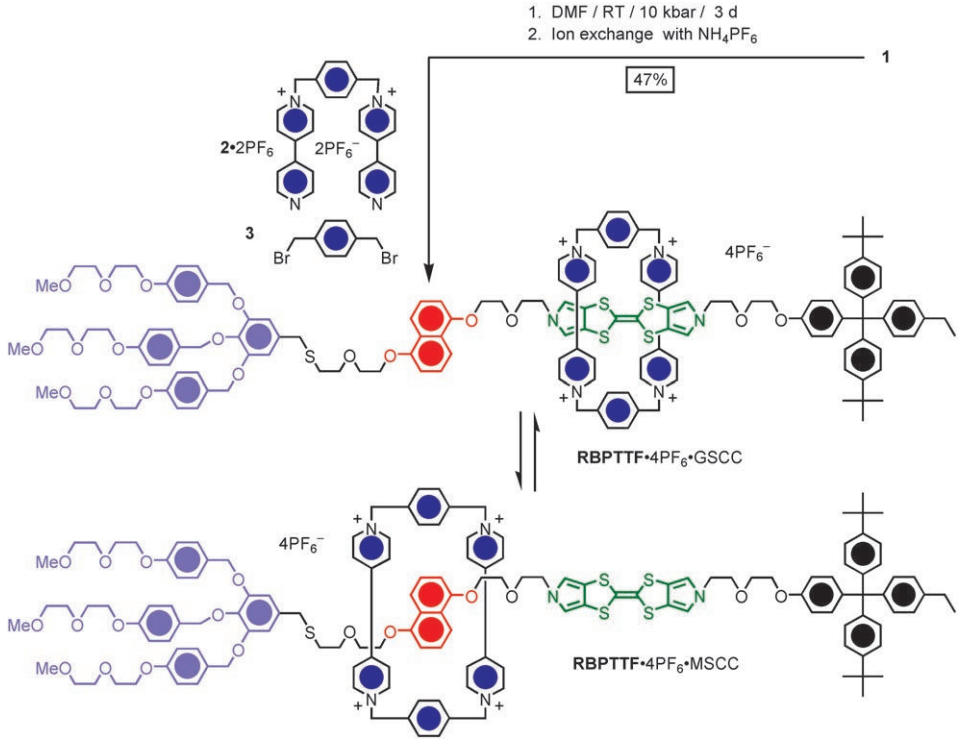

Scheme 3. Synthesis of the bistable [2]rotaxane RBPTTF·4 PF_6.

the ^{1}H NMR spectrum (400 MHz) recorded on RBPTTF·4 PF_6, since several protons in the dumbbell component give rise to two sets of signals, one for each of the two isomers. From integration of the resonances associated with the benzylic protons in the hydrophilic stoppers, the MSCC/GSCC equilibrium population ratio was found to be 1:3 at 295 K in CD_3CN.

Synthesis of the amphiphilic [2]rotaxane RBLOCK·4 PF_6: The [2]rotaxane RBLOCK·4 PF_6 was synthesized according to the routes outlined sequentially in Schemes 4 and 5. A solution of 4,5-bis(2-cyanoethylthio)-1,3-dithiole-2-thione[46] (**19**) in THF was treated with one equivalent of NaOMe. This procedure generated the monothiolate, which was alkylated with EtI affording compound **20** in 92% yield. Cross-coupling of 5-tosyl-(1,3)-dithiolo[4,5-*c*]pyrrole-2-one[43] (**21**) with three equivalents of the thione **20** in neat $(EtO)_3P$ gave (Scheme 4) the MPTTF derivative **22** (74%) in gram quantities after column chromatography. The iodide[28h] **18** was coupled with the MPTTF building block **22**, following its in situ deprotection with one equivalent of CsOH·H_2O to give **23** in 87% yield. The tosyl protecting group on the MPTTF unit was removed in good yield (87%) using NaOMe in a THF/MeOH mixture. The resultant pyrrole nitrogen atom in **24** was alkylated with compound **25**,[47] affording the chloride **26** in 75% yield. The chloride in compound **26** was initially converted to (**26**→**27**) an iodide in 99% yield and then to (**27**→**28**) a thiocyanate group in 99% yield. The thiocyanate group was reduced in situ with $NaBH_4$, and the resulting thiolate was subsequently coupled with the hydrophilic chloride[21] **17** in THF to give

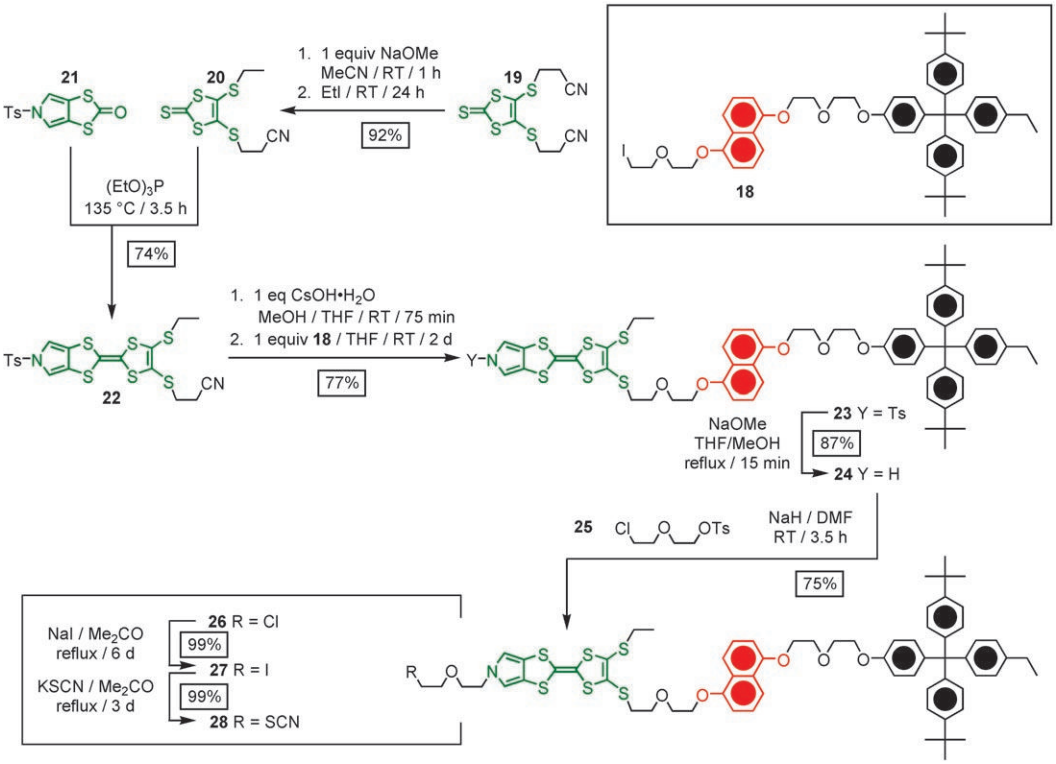

Scheme 4. Synthesis of the semi-dumbbell compound **28**.

the dumbbell **29** in 78% yield. Finally, the [2]rotaxane RBLOCK•4PF_6 was self-assembled (Scheme 5) under high-pressure conditions by using the dumbbell compound **29** as the template for the formation of the encircling $CBPQT^{4+}$ tetracation; the [2]rotaxane RBLOCK•4PF_6 was isolated in 41% yield from a mixture of the dumbbell compound **29**, the dicationic precursor[45] **2**•2PF_6, and the dibromide **3** after they had been subjected to a 10 kbar pressure in DMF at room temperature for three days.

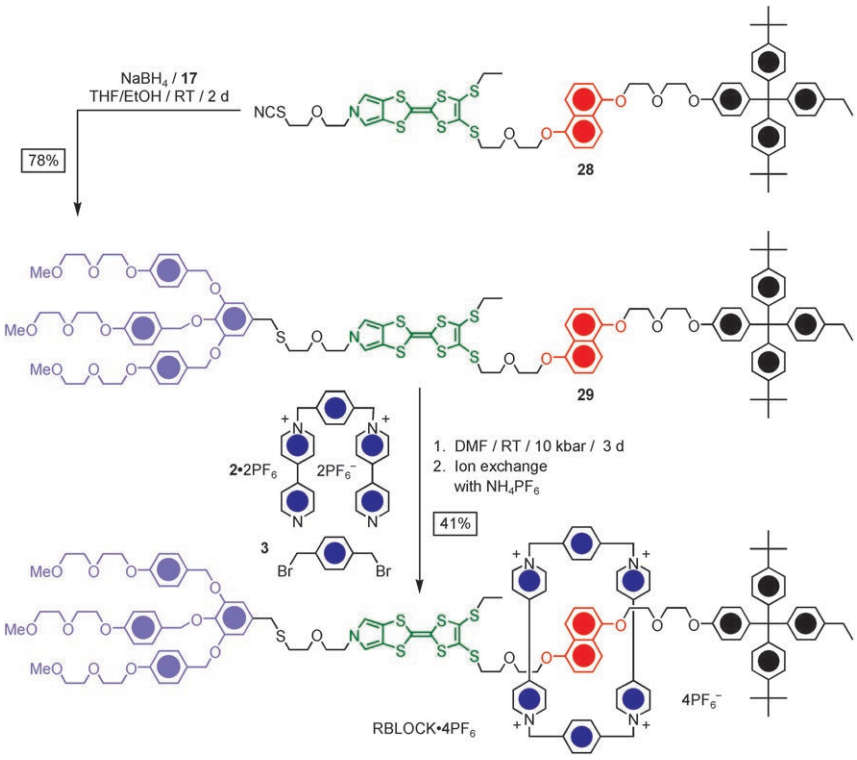

Scheme 5. Synthesis of the [2]rotaxane RBLOCK•4PF_6.

Kinetics and thermodynamics of switching in solution and in polymer electrolytes: We have previously demonstrated that the first oxidation potentials of bistable rotaxanes can be utilized to quantify the MSCC/GSCC ratios in the solution phase,[27] for monolayers assembled onto Au surfaces,[26] and for polymer electrolyte gels.[25] In this section, we report on a set of similar variable time and temperature cyclic voltammetry (VTTCV) measurements in solution and polymer environments to probe the thermodynamics of the MSCC/GSCC

equilibrium ratios for $RATTF^{4+}$ and $RBPTTF^{4+}$. From these measurements, we can extract free energy differences (ΔG from Figure 1b) between the two co-conformations.

We also utilized VTTCV to quantify the kinetics ($\Delta G^{\ddagger}$ from Figure 1b) associated with the recovery of the equilibrium MSCC/GSCC distribution for $RBPTTF^{4+}$ and $RATTF^{4+}$. The relaxation kinetics for [2]rotaxane $RATTF^{4+}$ and for related TTF-based rotaxanes were thoroughly investigated in recent papers,[25–27] while the equivalent VTTCV measurements for $RBPTTF^{4+}$ are reported here for the first time.

The VTTCV measurements were carried out as follows: two CV cycles were collected in succession, starting with the system at equilibrium. This first CV cycle displays peaks that can be assigned to the resting state populations of the MSCC and GSCC, since the first oxidation potential of the TTF (BPTTF) group is sensitive to whether or not it is encircled by the $CBPQT^{4+}$ ring. The second cycle, if collected quickly enough, records a shift in the equilibrium population towards the one dominated by the MSCC. This shift is reflected in an increase in the area of the peak assigned to the MSCC, in coincidence with a decrease in the area for the GSCC peak. By controlling the time between the first and second CV cycles, and the temperature of the experiment, the kinetic parameters associated with the recovery of the MSCC/GSCC equilibrium ratio can be quantified.

We first focus on utilizing VTTCV to probe the MSCC/GSCC population ratio at thermal equilibrium. The CVs of $RBPTTF^{4+}$ in the solution phase exhibit a peak at $+530$ mV, which corresponds to the $BPTTF \rightarrow BPTTF^{\cdot+}$ oxidation of the proportion of the bistable rotaxane that exists in the MSCC (Figure 4a). The smaller peak at $+680$ mV corresponds to the $BPTTF \rightarrow BPTTF^{\cdot+}$ oxidation of the GSCC. The larger peak at $+780$ mV corresponds to the second oxidation ($BPTTF^{\cdot+} \rightarrow BPTTF^{2+}$). This second oxidation is independent of the co-conformation, since once the $BPTTF^{\cdot+}$ is formed, the $CBPQT^{4+}$ ring moves to the DNP unit. The MSCC/GSCC population was thus measured as a function of temperature. For $RBPTTF^{4+}$, decreasing the temperature led to a significant increase in the MSCC/GSCC population ratio. The ratio, for example, increases (Figure 4a) more than two-fold (from around 0.3 to 0.7) as the temperature is decreased from 284 to 262 K. By comparison, for $RATTF^{4+}$, the MSCC/GSCC population ratio does not deviate significantly from 0.1, even when the rotaxane is probed (Figure 4b) over a broader temperature range (248–283 K).

The relative temperature dependences of the MSCC/GSCC ratios for $RBPTTF^{4+}$ and for $RATTF^{4+}$ are consistent with the ITC investigations of the complexation of the $CBPQT^{4+}$ host with the individual BPTTF-DEG, TTF-DEG, and DNP-DEG guests that were discussed above and presented in Table 1. Translating the behavior of the guests to what might be predicted for the two bistable [2]rotaxanes, one expects that the enthalpic contribution $\Delta H = (H_{MSCC} - H_{GSCC})$ should be significantly less than zero for $RBPTTF^{4+}$. By comparison, the corresponding ΔH for $RATTF^{4+}$ should be much closer to zero. As a consequence, the MSCC/GSCC ratio for $RBPTTF^{4+}$ varies[42] more readily with temperature.

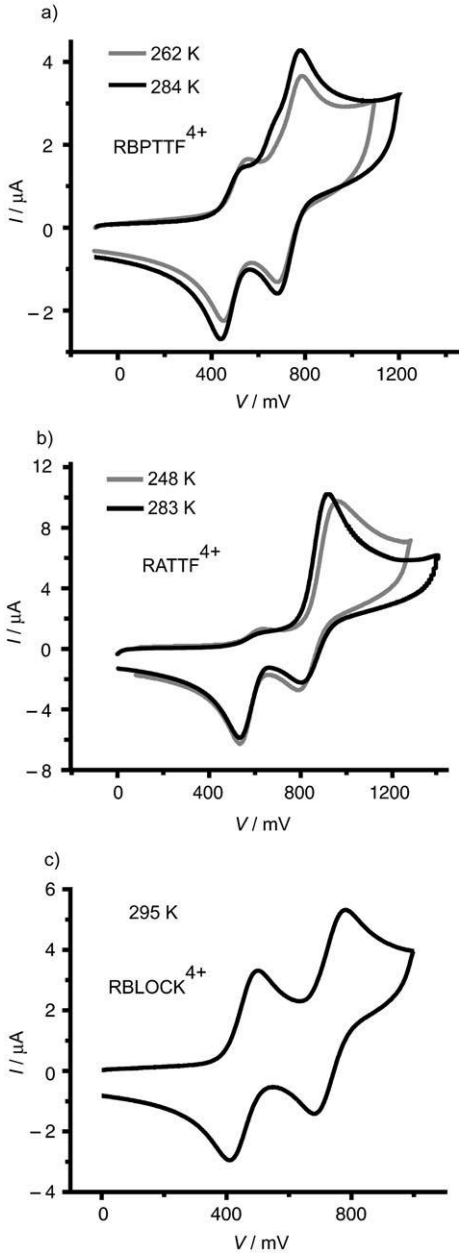

Figure 4. The first CV cycles of a) $RBPTTF^{4+}$ recorded at 262 and 284 K, b) $RATTF^{4+}$ recorded at 248 and 283 K, and c) $RBLOCK^{4+}$ recorded at 295 K (MeCN/0.1 M $TBAPF_6$/200 mV s^{-1}). The peak assigned to the MSCC at approximately $+500$ mV for $RBPTTF^{4+}$ fluctuates more than for $RATTF^{4+}$ across different temperature ranges. The simple, dumbbell-like CV for $RBLOCK^{4+}$, displaying a full-intensity MSCC peak at about 500 mV, verifies that the $CBPQT^{4+}$ ring is sterically blocked.

Although it is not so straightforward to interpret, the long and flexible diethylene glycol chains appear to have an impact on the binding K_a and therefore the population ratios of the bistable rotaxanes. The DEG chains enhance (Table 1) the binding affinity for each of the three guests

with the CBPQT^{4+} host, but they do so by influencing the ΔH and ΔS of each component differently. For TTF-DEG, the DEG chains leads to better enthalpy, but worse entropy. However, for the DNP-DEG and BPTTF-DEG guests, it is the opposite with the entropy contribution favoring binding and enthalpy disfavoring it, albeit only mildly so. Furthermore, it is known that when these DEG chains are attached to DNP and TTF units they are capable of wrapping themselves around the CBPQT^{4+} ring in order to acquire stabilizing, noncovalent C–H···O interactions.[37] Consequently, the significant enhancement of the enthalpic contribution to the complexation between TTF-DEG and the CBQPT^{4+} host by the DEG chains brings its ΔH to within a few kcal mol^{-1} of the DNP-DEG guest, leading to a relatively temperature-insensitive MSCC/GSCC ratio for the rotaxane RATTF^{4+}. However, the DEG chains have little effect on the ΔH contribution to complexation of the DNP-DEG and BPTTF-DEG guests by the CBPQT^{4+} host, such that they maintain their large and significant differences in enthalpy within the RBPTTF^{4+}, leading to the rotaxane's correspondingly large sensitivity of the population ratios to temperature. The DEG chains are thus an essential factor influencing the temperature sensitivities of the MSCC/GSCC population ratios of these bistable rotaxanes. The observation from the electrochemical studies in the solution phase and in the polymer matrix provide a view of both RATTF^{4+} and RBPTTF^{4+} that is completely consistent with the ITC measurements on the subunits of the rotaxanes. It is also consistent with the molecular structure differences between these two switches.

The relaxation kinetics and thermodynamics associated with the free-energy barrier ($\Delta G^{\neq}$) for relaxation from the MSCC to the GSCC for RATTF^{4+} and RBPTTF^{4+} were also analyzed quantitatively. The viscosity of the acetonitrile phase and polymer gel were about 3.5 cP and 50 000 cP at 298 K, respectively. This large increase in viscosity is reflected in the slower first-order decay kinetics for RBPTTF^{4+} as measured by VTTCV. Data for acetonitrile and the polymer gel are presented in Figure 5a and b, respectively. In addition to the viscosity effects, these plots also reveal how the thermally activated relaxation rates drop as the temperature is lowered. It's instructive to notice that both the MSCC and GSCC are at significant concentrations under equilibrium conditions for RBPTTF^{4+}, especially at lower temperatures. The implication is that the reverse reaction GSCC→MSCC is occurring at a rate comparable to that of the forward reaction. In analyzing the relaxation kinetics, both processes should be taken into consideration. Thus, for the equilibrium reaction given in Equation (1) the formula in Equation (2) is readily obtained (cf. Experimental Section), in which $x_t = N_{MSCC}/N_{Total}$ is the MSCC population ratio at time t, $x_0 = x_{t=0}$, and $x_{eq} = x_{t\to\infty}$ is the MSCC population ratio at final equilibrium.

$$\mathrm{MSCC} \underset{k_2}{\overset{k_1}{\rightleftharpoons}} \mathrm{GSCC} \qquad (1)$$

$$x_t = x_{eq} + (x_0 - x_{eq}) \exp[-k_1 t/(1-x_{eq})] \qquad (2)$$

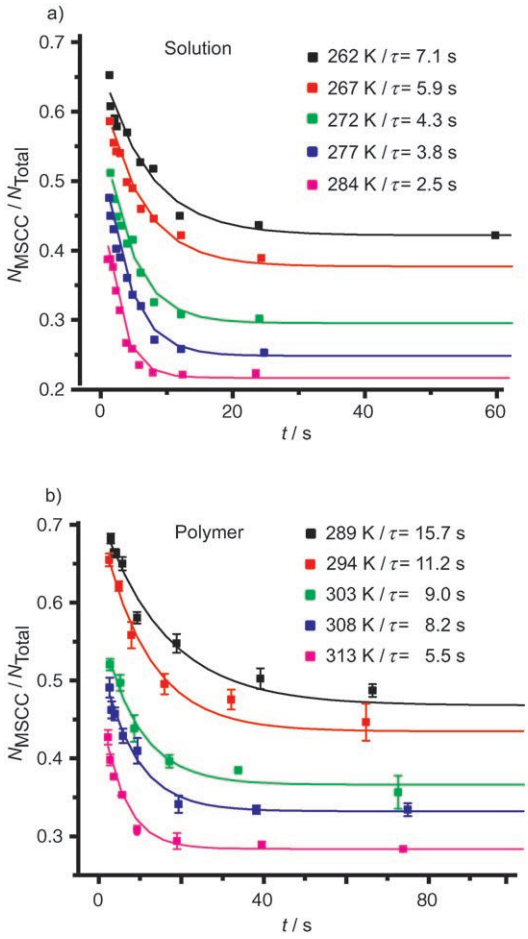

Figure 5. Fitted exponential decay curves and time constants (τ) obtained from the CV data for RBPTTF^{4+} measured at various scan rates for each temperature in a) solution and b) polymer phases.

Experimental relaxation data were thus fitted with this formula to obtain the decay time constant τ, and accordingly the rate constant for the forward reaction $k_1 = (1-x_{eq})/\tau$. Note that when x_{eq} is small (i.e., for the case of R(A)TTF^{4+}), the formula naturally reduces to the more familiar formula for a simple first-order reaction. The parameters $\Delta G^{\neq}$, $\Delta H^{\neq}$, $\Delta S^{\neq}$, and E_a were then fitted from the temperature dependence of k_1.[49,50] The kinetic data are summarized in Table 2 alongside values for R(A)TTF^{4+}. Note that the MSCC/GSCC population ratio for RBPTTF^{4+}, as measured at long times (at equilibrium), shows (Figure 5) a significant sensitivity to temperature that is consistent with the thermodynamic descriptions and data for the host–guest complexation. By contrast, RATTF^{4+} displays only a small thermal sensitivity in both the polymer and solution phase environments.

Kinetics and thermodynamics of molecular-switch tunnel junctions: The MSTJs investigated here contained a monolayer of the amphiphilic bistable rotaxanes RTTF^{4+} or RBPTTF^{4+}, or the sterically blocked metastable-like rotaxane RBLOCK^{4+}, sandwiched between an n-type poly-

Table 2. Kinetics data for the relaxation from the MSCC to the GSCC for $RBPTTF^{4+}$ and the free-energy barriers for $RATTF^{4+}$ and $RTTF^{4+}$. Data for solution, polymer and MSTJ were obtained from variable temperature CVs and from measurements of the relaxation of a MSTJ from the high to the low conductance state.[49,50]

	τ_{298} [s]	k_{298} [s^{-1}]	$\Delta G^{\ddagger}_{298}$ [kcal mol^{-1}]	$\Delta H^{\ddagger}$ [kcal mol^{-1}]	$\Delta S^{\ddagger}$ [cal $mol^{-1} K^{-1}$]	E_a [kcal mol^{-1}]	$\Delta G^{\ddagger}_{298}$ $RATTF^{4+}$	$\Delta G^{\ddagger}_{298}$ $RTTF^{4+}$
solution[a]	1.26 ± 0.10	0.69 ± 0.05	17.69 ± 0.05	8.4 ± 0.5	-31.0 ± 1.7	9.0 ± 0.5	16.2 ± 0.3	–
polymer[b]	10.2 ± 0.12	0.059 ± 0.001	19.15 ± 0.01	8.4 ± 1.1	-36.0 ± 3.4	9.0 ± 1.0	18.1 ± 0.2	–
MSTJ	624 ± 82	$(8.4 \pm 0.8) \times 10^{-4}$	21.7 ± 0.1	16.1 ± 1.4	-18.7 ± 4.1	16.7 ± 1.3	–	22.21 ± 0.04

[a] Solution-phase data was obtained for 1 mM samples dissolved in MeCN (0.1 M $TBAPF_6$) using a glassy carbon working electrode. All potentials were referenced to a Ag/AgCl reference electrode.[27] [b] Polymer-phase data was obtained in a polymer matrix—*w*:*w*:*w*:*w* ratios of 70:7:20:3 for MeCN/polymethylmethacrylate/propylene carbonate/$LiClO_4$. The sample was spread onto three lithographically patterned Pt electrodes (50 nm) on top of Ti (10 nm) (working, counter, reference).[25] The $\Delta H^{\ddagger}$ and $\Delta S^{\ddagger}$ were obtained from an average of many devices, while the Eyring plot in Figure 8b represents just one device.

(silicon) bottom electrode (passivated with the native oxide) and a metallic top electrode. The detailed procedures relating to the fabrication and operation of these devices have been previously reported.[20–22] Briefly, the molecules are prepared as a Langmuir–Blodgett film and then transferred as a compressed Langmuir monolayer ($\pi = 30$ mN m^{-1}) onto a substrate pre-patterned with poly-silicon electrodes. A thin 10 nm Ti adhesion layer, followed by a thicker 200 nm top Al layer is evaporated through a shadow mask by using e-beam evaporation to form the top electrodes. During this step, the substrate is held at room temperature at a source–sample distance of ~0.7 m. This procedure ensures that little or no substrate heating from the e-beam evaporation source occurs. The e-beam evaporation was processed at the deposition rate of 1–2 Å s^{-1} under high vacuum (~5×10^{-7} Torr). For all experiments reported here, the bottom electrodes were 5 μm wide, n-type (doping level ~5×10^{-19} cm^{-3}) poly-Si, while the top electrodes were 10 μm wide. Each fabrication run produced approximately 100 MSTJ devices, and the results presented here were consistently observed in multiple devices across multiple fabrication runs, with temperature-dependent data collected in random sequence. More than 90% of the MSTJ devices displayed consistent and reproducible temperature dependence. The operational characteristics of MSTJs containing bistable catenanes and rotaxanes, but patterned at both larger and also much smaller dimensions, have been reported.[22,24]

CV measurements are not possible for MSTJs, but there are other electronic measurements that can be carried out to assess both the thermodynamic and kinetic properties of the bistable rotaxanes within the devices. Our hypothesis—for both bistable catenanes and bistable rotaxanes—has been refined such that the MSCC represents the high-conducting, switch-closed state of the device, while the MSCC/GSCC ratio at equilibrium represents the low-conducting, switch-open state. For an MSCC-dominated system, regardless of environment, reduction of the $CBPQT^{4+}$ ring provides a rapid route towards recovering the equilibrium MSCC/GSCC distribution.[20,26] In the absence of such a reduction step, a device in the high-conductance state will relax to the equilibrium MSCC/GSCC ratio, according to a timescale described by $\Delta G^{\ddagger}$ (Figure 1b). From a practical point of view (i.e., for memory devices), this relaxation process correlates to the volatility, or memory-retention characteristics, of the device. The volatility can be quantified by measuring the temperature dependence of the decay of the switch-closed, high-conductance state of a device back to the switch-open state.

The equilibrium thermodynamic properties of the devices can also be inferred within MSTJs by considering that the high- and low-conductance states of the devices correlate with different MSCC/GSCC ratios. Thus, the temperature-dependent switching amplitude, normalized against the temperature-dependent transport characteristics of an MSTJ, opens a window into the thermodynamics of the molecules within the junction. Such a measurement provides a qualitative picture that can be compared against quantitative VTTCV measurements of the MSCC/GSCC ratios in other environments.

Measurements of the bistable character of MSTJs containing $RTTF^{4+}$, $RBTTF^{4+}$, and the $RBLOCK^{4+}$ control rotaxane are shown in Figure 6a and b. This type of data is called a remnant molecular signature,[20–22] and represents a nearly capacitance-free map of the hysteretic response of an MSTJ. Briefly, the *x* axis of a remnant molecular signature plot correlates to a value of a voltage pulse that is applied across the junction. A train of voltage pulses, starting at 0 V and following the direction of the arrows shown on the plots, is applied to the MSTJ, and, after each voltage pulse, the current through the MSTJ is monitored at +0.1 V.[51] The resulting normalized current is represented on the *y* axis. These hysteresis loops not only provide a key indicator that the MSTJs can be switched reversibly between the high- and low-conducting states, but they also qualitatively reflect the ground-state MSCC/GSCC ratio, since the switching amplitude is sensitive to this ratio. For the high-conductance state, in which the entire population has been converted into the MSCC, the maximum current is controlled by the intrinsic conductance properties of this co-conformation. However, for the low-conductance state, the minimum conduction is not only controlled by the intrinsic properties of the GSCC but also by the MSCC/GSCC ratio—a factor under thermodynamic control. For instance, at 295 K $RBPTTF^{4+}$ and $RBLOCK^{4+}$ do not appear to be "good" switches, while the switching amplitude of $RTTF^{4+}$ is about a factor of 8. At 320 K, the small hysteretic response for $RBLOCK^{4+}$ dimin-

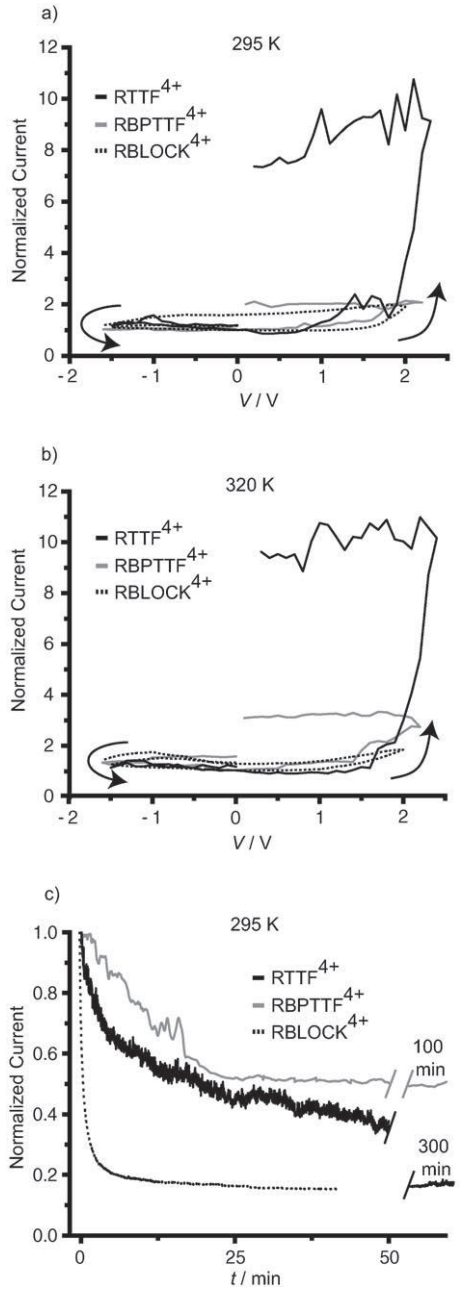

Figure 6. Switching responses of three rotaxanes within MSTJs. a) and b): Remnant molecular signature traces of the hysteretic switching responses. The arrows indicate the direction of the voltage sweep, and all currents were recorded at +0.1 V. The *y* axis current was normalized by setting the initial (low-conductance state) current to 1. Note that the response of $RBPTTF^{4+}$ increases in amplitude at higher temperature, reflecting a decreasing MSCC/GSCC equilibrium ratio, while $RTTF^{4+}$ is relatively constant. There is a finite amount of field-induced polarization in $RBLOCK^{4+}$ that is almost undetectable at 320 K. c) Relaxation of MSTJs from high-to-low conducting states recorded at 295 K. The characteristic relaxation times are: $RTTF^{4+}$ = 3450 s; $RBPTTF^{4+}$ = 660 s; $RBLOCK^{4+}$ = 60 s.

ishes further, but the hysteresis loop of $RBPTTF^{4+}$ opens up to yield a switching amplitude (i.e., the current measured in the high conductance state divided by the current measured in the low conductance state) of over 3. This enhanced switching amplitude presumably reflects a smaller MSCC/GSCC equilibrium ratio at the higher temperature, and is consistent with what is observed for the solution and polymer phase measurements for $RBPTTF^{4+}$. The switching amplitude of $RTTF^{4+}$ remains fairly constant across this temperature range, consistent again with measurements in the other environments. The MSCC→GSCC relaxation kinetics can be monitored by measuring the time-dependence of the decay of the high-conductance to the low-conductance state; the data for all three amphiphilic rotaxanes at 295 K is presented in Figure 6c.

The high- to low-conductance decay of all three rotaxanes exhibited different temperature dependences. While MSTJs fabricated from $RBPTTF^{4+}$ and $RTTF^{4+}$ show strong temperature dependences—as the temperature was increased from 295 K to 320 K, the 1/e decay time decreased by factors of 6–7 for those rotaxanes (Figure 7)—$RBLOCK^{4+}$ exhibited a much weaker temperature dependence. MSTJs fabricated from $RBLOCK^{4+}$ were investigated over a

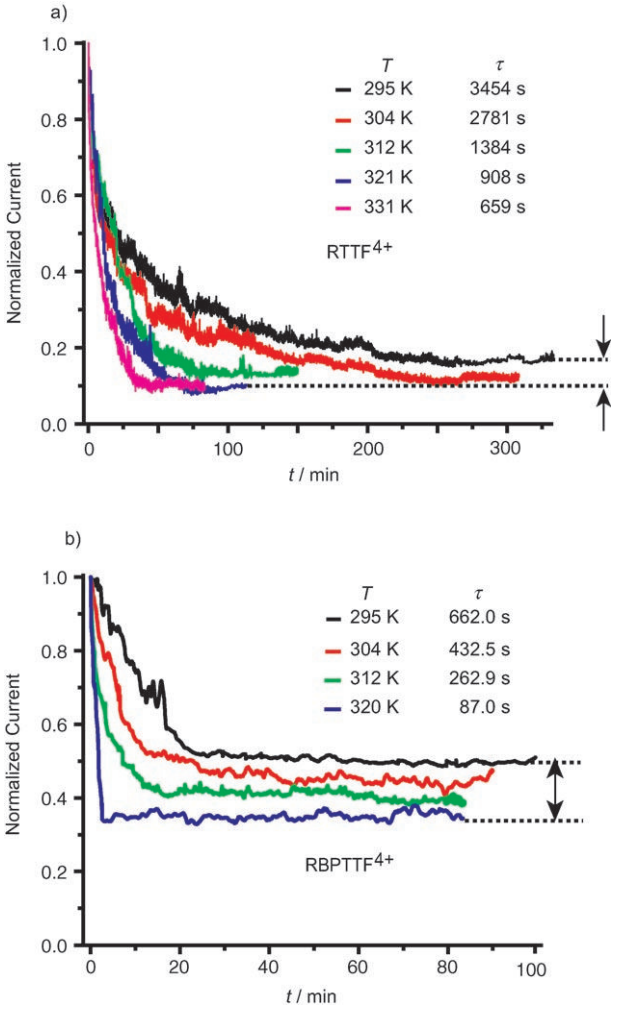

Figure 7. Decay curves of a) $RTTF^{4+}$ and b) $RBPTTF^{4+}$ MSTJs recorded as a function of temperature. Note that the normalized switching amplitude of $RBPTTF^{4+}$ exhibits a strong temperature dependence.

broader temperature range (295–383 K) and the characteristic relaxation time decreased by only a factor of 2 or so over this entire range. This decay-rate data fitted well to a $1/T$ plot ($R^2 > 0.99$), which is at least consistent with existing models for dielectric relaxation,[52,53] although measurements over an even broader temperature range would be required to establish this relationship more firmly. In any case, MSTJs fabricated from RBLOCK^{4+} were poor switches at all temperatures investigated, and the small switching response that could be recorded exhibited a very different and much less-pronounced temperature dependence, in comparison to MSTJs fabricated from RBPTTF^{4+} and RTTF^{4+}.

The switching amplitude can be recorded by either measuring the amplitude of the hysteresis loops from the remnant molecular signature data, or by measuring the time-dependent decay of the high- to the low-conductance state. Any molecular electronic junction for which charge transport is not strictly a quantum mechanical tunneling process will exhibit a strong temperature-dependent conductance, that is, charge transport is thermally activated, and the rate of transport increases with increasing temperature. This is the case for all three of the amphiphilic rotaxanes investigated here. However, this temperature-dependent component should depend only weakly upon molecular structure, especially for molecules that are as similar as RTTF^{4+}, RBPTTF^{4+}, and RBLOCK^{4+}, and should not be particularly sensitive to the MSCC/GSCC ratio within a device. Thus, we remove this component of the temperature dependence by normalizing the switching amplitude to the initial current value, measured at $t=0$ after placing the switch into the high conductance state. The hypothesis is that the (normalized) current at long times—that is, when the system has reached equilibrium—divided by the $t=0$ current should correlate[54] qualitatively with the MSCC/GSCC ratio. In Figure 7, we present such normalized decay curves, for various temperatures, for both RTTF^{4+} and RBPTTF^{4+}. Note two things about the data of Figure 7. First, the curves clearly represent activated processes, since, for both bistable rotaxanes, the relaxation times decrease rapidly with increasing temperature. Second, the switching amplitude for RTTF^{4+} is relatively temperature independent, exhibiting almost an order-of-magnitude difference in the (normalized) current change between the high- and low-conductance states for all temperatures. By contrast, the switching amplitude for RBPTTF^{4+} exhibits a strong temperature dependence over the same range. This observation is consistent with the remnant molecular signature data presented in Figure 6. Also, it is consistent with the behavior of the corresponding bistable rotaxanes (RATTF^{4+} and RBPTTF^{4+}) in the other environments, as well as the ITC data obtained from host-guest complexation experiments.

The temperature-dependent thermodynamic and relaxation kinetic data for all environments are presented in Figure 8a and b, respectively. In Figure 8a, we have plotted the temperature-dependent ratios as N_{MSCC}/N_{TOTAL}, quantitatively measured in the solution-phase and polymer environments. For the MSTJs, this ratio cannot be quantified, but

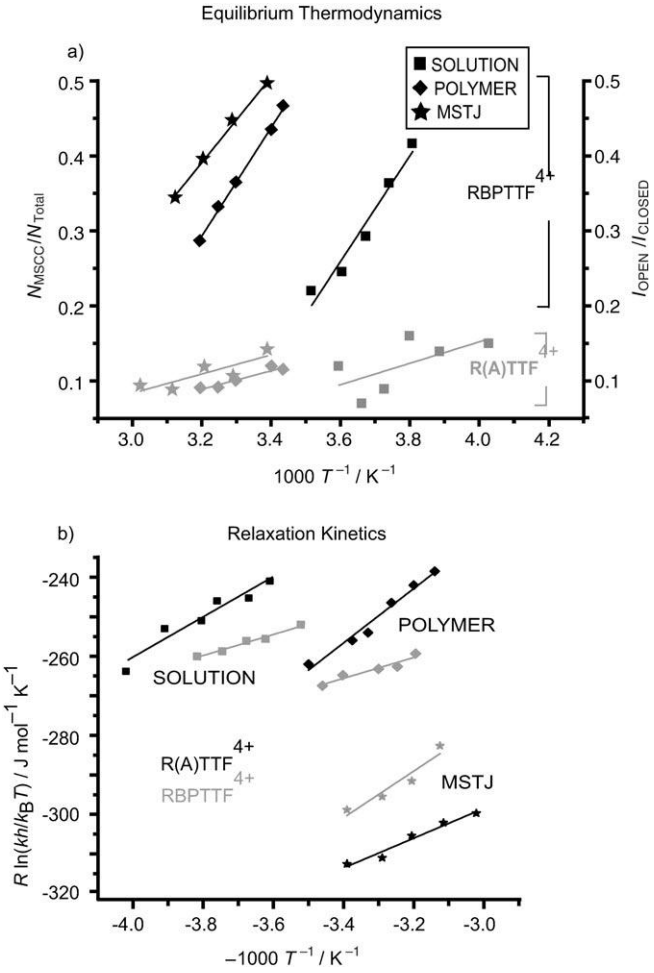

Figure 8. a) The temperature-dependent GSCC/MSCC equilibria for all three environments are presented. Solution and polymer phase data (N_{MSCC}/N_{Total}) were recorded for RATTF^{4+} and RBPTTF^{4+} and are based upon quantitative electrochemical measurements of the MSCC/GSCC ratios. The MSTJ data, which were recorded for RTTF^{4+} and RBPTTF^{4+}, show the temperature-dependent switching amplitude (I_{OPEN}/I_{CLOSED}), and represent a qualitative measurement of the N_{MSCC}/N_{Total} ratio, based upon the proposed switching mechanism. Note that the large (enthalpically driven) temperature dependence for RBPTTF^{4+}, and the relative temperature independence of RATTF^{4+} and RTTF^{4+} (R(A)TTF^{4+}) is reflected in all environments. b) Eyring plots of the MSCC→GSCC (or high→low-conducting MSTJ) relaxation process, for all three environments.

the temperature-dependent switching amplitude I_{OPEN}/I_{CLOSED} provides for qualitative comparison[54] with the other environments. For the relaxation kinetics, data for the two TTF-containing rotaxanes (R(A)TTF^{4+} and RBPTTF^{4+}) are plotted in the form of Eyring plots, in order to quantify (Table 2) $\Delta G^{\ddagger}$, $\Delta H^{\ddagger}$, and $\Delta S^{\ddagger}$ in all three environments.[49,50]

We first consider the kinetic data given in Figure 8b and Table 2. For the case of RBPTTF^{4+}, the free-energy barrier ($\Delta G^{\ddagger}$) to relaxation at 298 K increases from 17.7 to 19.2 to 21.7 kcal mol^{-1} upon moving from acetonitrile to polymer gels to MSTJs. For R(A)TTF^{4+}, the situation is qualitatively similar. Both rotaxanes exhibit an increase in the energy barrier $\Delta G^{\ddagger}$ from the solution to polymer phase by between

1 and 2 kcal mol^{-1}. However, the $\Delta G^{\ddagger}$ increase in moving from the polymer to the MSTJ is significantly larger for R(A)TTF^{4+} than for RBPTTF^{4+} (4.1 vs 2.5 kcal mol^{-1}). This difference may be related to the differences in packing between the Langmuir monolayers of the amphiphilic rotaxanes. Both monolayers were transferred onto the electrode-patterned substrate at a pressure of 30 mN m^{-1}. However, the RTTF^{4+} rotaxanes occupy 92 ± 3 Å^2 per molecule, while the RBPTTF^{4+} rotaxanes occupy 122 ± 5 Å^2 per molecule. Thus, the packing of RBPTTF^{4+} is influenced by a combination of the high MSCC/GSCC ratio and the bulkier hydrophilic stopper. These differences lead to a 30% increase in the area per molecule over a similarly compressed film of RTTF^{4+}. Nevertheless, for both amphiphilic bistable rotaxanes, the data in Figures 6 and 7 indicate a qualitatively similar switching mechanism, regardless of physical environment.

The thermodynamic data given in Figure 8a are apparently more reflective of the structural differences between R(A)TTF^{4+} and RBPTTF^{4+}, rather than the physical environment of these molecules. In all environments, RBPTTF^{4+} exhibits a strongly temperature-dependent switching amplitude that can be related back to the temperature dependence of the MSCC/GSCC ratio. In turn, this behavior can be connected to the free-energy difference between the two host–guest complexes, BPTTF-DEG⊂CBPQT^{4+} and DNP-DEG⊂CBPQT^{4+}, and the fact that the enthalpic contribution to the free energy is very different for these two complexes. The temperature dependence of the MSCC/GSCC ratio of RBPTTF^{4+} is slightly more pronounced for the solution and polymer environments than for the MSTJ. This is likely due to the fact that the MSTJ constitutes a more sterically crowded environment. Nevertheless, the degree to which the free-energy landscape of the bistable RBPTTF^{4+} is reflected in the properties of this molecule, regardless of environment, is striking.

In a similar way, the temperature independent switching amplitude of R(A)TTF^{4+} can also be rationalized within a self-consistent picture that connects across all environments as well as to the free-energy differences between the TTF-DEG⊂CBPQT^{4+} and DNP-DEG⊂CBPQT^{4+} host–guest complexes. From the point of view of an MSTJ-based memory device, RTTF^{4+} constitutes a much superior switch than does RBPTTF^{4+}. First, it exhibits a stable switching amplitude over a reasonably broad temperature range. Second, an RTTF^{4+}-based MSTJ remains in the high-conducting (MSCC-dominated) state five times longer than an RBPTTF^{4+}-based MSTJ at 295 K, and ten times longer at 320 K, implying a less volatile (and more useful) switch.

Conclusion

We have investigated two classes of bistable rotaxanes—one containing a TTF unit and the other a BPTTF unit—across different environments. Quantifying the relaxation rates in one critical step of the switching cycle enables us, not only to validate the proposed switching mechanism and its universality, but also to correlate switching speeds with the nature of the environment. The trends in the kinetics and the validity of the switching mechanism hold true for both classes of bistable rotaxanes. Nevertheless, we are still able to differentiate them by following a detailed thermodynamic investigation of their thermally equilibrated states. By replacing the TTF unit in the bistable rotaxanes with a BPTTF unit, the equilibrium MSCC/GSCC population ratio, which influences the low-conductance state in MSTJs and the temperature sensitivity of this ratio, was altered considerably. Correspondingly, the switching amplitude between the high-conductance state and the now thermally sensitive low-conductance state changes significantly with temperature. Binding constant measurements for the complexation of model guests with the CBPQT^{4+} host verify that the population ratio and its temperature sensitivity are directly related to the different binding strengths of the DEG-disubstituted TTF and BPTTF units. Enthalpy is found to play a crucial role in determining the temperature dependence of these binding strengths. The observation of a mode of thermodynamic behavior that is universal regardless of environment validates the hypothesis that at least certain key operational characteristics of the MSTJs are under the control of chemical synthesis. This realization represents a key element in the emerging paradigm of molecular electronics.

Experimental Section

General methods: Chemicals were purchased from Aldrich and were used as received, unless indicated otherwise. Bis(pyrrolo[3,4-*d*])tetrathiafulvalene[43] (**4**; Scheme 1), 2-(2-iododethoxy)-ethyl-*p*-toluenesulfonate[44] (**5**; Scheme 1), 4-[bis(4-*tert*-butylphenyl)(4-ethylphenyl)methyl]phenol[21] (**9**; Scheme 1), compound[28d] **12** (Scheme 1), the chloride[21] **17** (Scheme 2 and 4), 1,1′′-[1,4-phenylenebis(methylene)]bis(4,4′-bipyridin-1-ium) bis(hexafluorophosphate)[45] (**16**·2 PF_6) (Schemes 3 and 5), the iodide[28h] **18** (Scheme 4), 4,5-bis(2-cyanoethylthio)-1,3-dithiole-2-thione[46] (**19**; Scheme 4), 5-tosyl-(1,3)-dithiolo-[4,5-*c*]pyrrole-2-one[43] (**21**; Scheme 4), and 2-(2-chloroethoxy)-ethyl-*p*-toluenesulfonate[47] (**25**; Scheme 4) were all prepared according to literature procedures. Solvents were dried according to literature procedures.[48] All reactions were carried out under an anhydrous nitrogen atmosphere. High-pressure experiments were carried out in a teflon tube on a Psika high-pressure apparatus. Thin-layer chromatography (TLC) was carried out by using aluminium sheets precoated with silica gel 60F (Merck 5554). The plates were inspected under UV light and, if required, developed in I_2 vapor. Column chromatography was carried out using silica gel 60F (Merck 9385, 0.040–0.063 mm). Deactivated SiO_2 was prepared by stirring the silica gel in CH_2Cl_2 containing 2% Et_3N for 10 min before it was filtered, washed with CH_2Cl_2, and dried. Melting points were determined on a Büchi melting point apparatus and are uncorrected. ^{1}H NMR spectra were recorded at room temperature on a Bruker ARX500 spectrometer (500 MHz), Bruker ARX400 spectrometer (400 MHz), or on a Gemini-300BB instrument (300 MHz), with residual solvent as the internal standard. ^{13}C NMR spectra were recorded at room temperature on a Gemini-300BB instrument (75 MHz), with residual solvent as the internal standard. ^{19}F NMR spectra were recorded at room temperature on a Bruker ARX400 spectrometer (376 MHz), while ^{31}P NMR spectra were recorded at room temperature on Bruker ARX400 instrument (161 MHz). All chemical shifts are quoted on a δ scale, and all coupling constants (J) are expressed in Hertz (Hz). The following abbreviations are used in listing the NMR spectra:

s = singlet, d = doublet, t = triplet, q = quartet, brs = broad singlet, and m = multiplet. Samples were prepared in $CDCl_3$, CD_3COCD_3, or CD_3SOCD_3 purchased from Cambridge Isotope Labs. Electron impact ionization mass spectrometry (EI-MS) was performed on a Varian MAT 311 A instrument and matrix-assisted laser-desorption/ionization time-of-flight mass spectrometry (MALDI-TOF-MS) was performed on a Kratos Kompact MALDI-TOF instrument, utilizing a 2,5-dihydroxybenzoic acid matrix, high-resolution Fourier Transform matrix-assisted laser-desorption/ionisation mass spectrometry (HiRes-FT-MALDI-MS) was performed on an IonSpec 4.7 tesla Ultima Fourier Transform mass spectrometer, utilizing a 2,5-dihydroxybenzoic acid (DHP) matrix, while electrospray mass spectra (ES-MS) were obtained from a from a Sciex API III$^+$ mass spectrometer. Infrared (IR) spectra were recorded on a Perkin–Elmer 580 spectrophotometer. UV-visible spectra were recorded at room temperature on a Shimadzu UV-160 instrument. Microanalyses were performed by the Atlantic Microlab, Inc., Atlanta, Georgia.

Compound 6: Compound **4** (0.80 g, 2.83 mmol) was dissolved in anhydrous DMF (30 mL), cooled to 0 °C, and degassed (N_2, 10 min) before the iodide **5** (2.50 g, 8.33 mmol) followed by NaH (0.80 g of a 60 % suspension in mineral oil, 20.0 mmol) was added to the yellow solution. The reaction mixture was stirred for 3 h at 0 °C, whereupon the reaction mixture was diluted with CH_2Cl_2 (500 mL), washed with brine (10 × 150 mL), and dried ($MgSO_4$). Removal of the solvent gave a brown oil that was purified by column chromatography (deactivated SiO_2: CH_2Cl_2/MeOH 19:1). The broad yellow band (R_f = 0.6) was collected and concentrated, affording compound **6** (1.19 g, 67 %) as a yellow oil. ^{1}H NMR (300 MHz, CD_3SOCD_3): δ = 1.40–1.80 (m, 12H), 3.40–4.00 (m, 20H), 4.54 (brs, 2H), 6.82 ppm (s, 4H); ^{13}C NMR (75 MHz, CD_3SOCD_3): δ = 19.6, 25.6, 30.8, 50.3, 61.7, 66.4, 70.1, 70.7, 98.5, 114.2, 117.2, 119.5 ppm; MS(EI): *m*/*z* (%): 626 (24) [M^+], 542 (18), 458 (10); elemental analysis calcd (%) for $C_{28}H_{38}N_2O_6S_4$: C 53.65, H 6.11, N 4.47; found: C 53.78, H 6.09, N 4.43.

Compound 7: A solution of compound **6** (1.14 g, 1.82 mmol) in THF/EtOH (50 mL, 1:1 v/v) was degassed (N_2, 10 min) before TsOH·H_2O (~10 mg, cat.) was added. The yellow solution was stirred for 20 h at room temperature, whereupon it was diluted with CH_2Cl_2 (100 mL). The combined organic phase was washed with a saturated aqueous $NaHCO_3$ solution (200 mL), H_2O (300 mL) and dried ($MgSO_4$). Concentration in vacuo gave a yellow powder, which was subjected to column chromatography (deactivated SiO_2: CH_2Cl_2/MeOH 24:1). The greenish yellow band (R_f = 0.3) was collected and the solvent evaporated to give compound **7** (0.56 g, 67 %) as a yellow powder. M.p. 138–139 °C; ^{1}H NMR (300 MHz, CD_3SOCD_3): δ = 3.39–3.42 (m, 8H), 3.64 (t, ^3J(H,H) = 5.2 Hz, 4H), 4.00 (t, ^3J(H,H) = 5.2 Hz, 4H), 4.59 (t, ^3J(H,H) = 5.2 Hz, 2H), 6.82 ppm (s, 4H); ^{13}C NMR (75 MHz, CD_3SOCD_3): δ = 49.8, 60.2, 70.2, 72.2, 113.7, 116.7, 118.9 ppm; MS(MALDI-TOF): *m*/*z* (%): 458 (100) [M^+]; elemental analysis calcd (%) for $C_{18}H_{22}N_2O_4S_4$: C 47.14, H 4.83, N 6.11, S 27.97; found: C 47.04, H 4.83, N 6.08, S 27.73.

Compound 8: TsCl (0.57 g, 2.99 mmol) dissolved in anhydrous CH_2Cl_2 (30 mL) was added dropwise over 20–30 min to an ice-cooled solution of the diol **7** (1.30 g, 2.83 mmol), Et_3N (2 mL, 1.5 g, 14 mmol), and 4-dimethylaminopyridine (DMAP; ~10 mg, cat.) in anhydrous CH_2Cl_2 (90 mL). The reaction mixture was stirred for 20 h (0 °C to RT), whereupon Al_2O_3 (10 g, Brockmann 1, neutral) was added and the solvent removed. The resulting green powder was directly subjected to column chromatography (deactivated SiO_2) and the bistosylate (0.90 g, 41 %) was eluted with CH_2Cl_2, whereupon the eluent was changed to CH_2Cl_2/MeOH (99:1) and the yellow band (R_f = 0.5) containing the desired monotosylate was collected and concentrated to give compound **8** (0.38 g, 22 %) as a yellow solid. Finally, the starting material **7** (0.45 g, 34 %) was eluted CH_2Cl_2/MeOH (23:2). ^{1}H NMR (300 MHz, CD_3SOCD_3): δ = 2.42 (s, 3H), 3.36–3.66 (m, 10H), 3.93–4.11 (m, 6H), 4.59 (t, ^3J(H,H) = 5.2 Hz, 1H), 6.74 (s, 2H), 6.83 (s, 2H), 7.46 (d, ^3J(H,H) = 8.0 Hz, 2H), 7.75 ppm (d, ^3J(H,H) = 8.0 Hz, 2H); ^{13}C NMR (75 MHz, CD_3SOCD_3): δ = 21.1, 49.5, 49.7, 60.2, 67.7, 69.8, 70.1, 70.2, 72.1, 113.6, 113.7, 116.7, 116.8, 118.9, 127.6, 130.1, 132.5, 144.9 ppm (one line is missing/overlapping); MS(MALDI-TOF): *m*/*z* (%): 612 (100) [M^+]; elemental analysis calcd (%) for $C_{25}H_{28}N_2O_6S_5$: C 49.00, H 4.61, N 4.57, S 26.16; found: C 48.83, H 4.66, N 4.67, S 25.97.

Compound 10: A solution of the monotosylate **8** (0.37 g, 0.60 mmol) and **9** (0.86 g, 1.80 mmol) in anhydrous MeCN (50 mL) containing K_2CO_3 (0.50 g, 3.6 mmol), LiBr (10 mg, cat.) and [18]crown-6 (~10 mg, cat.), was heated at 75 °C for 20 h. After cooling down to room temperature, the reaction mixture was filtered and the residue washed thoroughly with MeCN (20 mL). The combined organic phase filtrate was concentrated in vacuo and the yellow residue was purified by column chromatography (deactivated SiO_2: CH_2Cl_2/Me_2CO 97:3). The yellow band (R_f = 0.2) was collected and the solvent evaporated to give compound **10** (0.38 g, 70 %) as a yellow foam. ^{1}H NMR (300 MHz, CD_3SOCD_3): δ = 1.17 (t, ^3J(H,H) = 7.6 Hz, 3H), 1.26 (s, 18H), 2.53 (q, ^3J(H,H) = 7.6 Hz, 2H), 3.39–3.49 (m, 4H), 3.62–3.71 (m, 6H), 3.99–4.02 (m, 6H), 4.59 (t, ^3J(H,H) = 5.2 Hz, 1H), 6.80–6.84 (m, 6H), 7.01–7.12 (m, 10H), 7.28–7.31 ppm (m, 4H); MS(EI): *m*/*z* (%): 917 (55) [M^+], 105 (100); elemental analysis calcd (%) for $C_{53}H_{60}N_2O_4S_4$: C 69.39, H 3.05, N 6.59, S 13.98; found: C 69.63, H 2.91, N 6.63, S 13.73.

Compound 11: A solution of compound **10** (0.38 g, 0.41 mmol), TsCl (0.16 g, 0.82 mmol), Et_3N (0.5 mL, 0.35 g, 3.3 mmol), and DMAP (~10 mg, cat.) in anhydrous CH_2Cl_2 (150 mL) was stirred at room temperature for 20 h. Al_2O_3 (10 g, Brockmann 1, neutral) was added, whereupon the solvent was removed and the residue was purified by column chromatography (deactivated SiO_2: CH_2Cl_2/Me_2CO 99:1). The yellow band (R_f = 0.15) was collected and the solvent evaporated to give compound **11** (0.35 g, 81 %) as a yellow foam. ^{1}H NMR (300 MHz, CD_3COCD_3): δ = 1.18 (t, ^3J(H,H) = 7.5 Hz, 3H), 1.29 (s, 18H), 2.43 (s, 3H), 2.60 (q, ^3J(H,H) = 7.5 Hz, 2H), 3.61–3.66 (m, 4H), 3.75–3.79 (m, 4H), 3.98–4.16 (m, 8H), 6.64 (s, 2H), 6.73 (s, 2H), 6.81 (d, ^3J(H,H) = 9.0 Hz, 2H), 7.09–7.15 (m, 10H), 7.28–7.32 (m, 4H), 7.45 (d, ^3J(H,H) = 8.4 Hz, 2H), 7.78 ppm (d, ^3J(H,H) = 8.4 Hz, 2H); MS(FT-MALDI): *m*/*z* (%): 1093 (2) [M^++Na], 1070 (100) [M^+], 921 (15); elemental analysis calcd (%) for $C_{60}H_{66}N_2O_6S_5$: C 67.26, H 6.21, N 2.61, S 14.96; found: C 65.78, H 6.24, N 2.36, S 14.91.

Compound 13: A solution of the tosylate **11** (0.64 g, 0.60 mmol) and **12** (0.26 g, 0.79 mmol) in anhydrous MeCN (50 mL) containing K_2CO_3 (0.34 g, 2.4 mmol), LiBr (10 mg, cat.) and [18]crown-6 (~10 mg, cat.) was heated under reflux for 20 h. After cooling down to room temperature, the reaction mixture was filtered and the residue washed with MeCN (2 × 50 mL). The combined organic phase filtrate was concentrated in vacuo and the yellow oily residue was purified by column chromatography (deactivated SiO_2: CH_2Cl_2/EtOH 97:3). The yellow band was collected and the solvent evaporated affording compound **13** (0.44 g, 60 %) as a yellow foam. ^{1}H NMR (300 MHz, CD_3COCD_3): δ = 1.20 (t, ^3J(H,H) = 7.6 Hz, 3H), 1.29 (s, 18H), 1.49–1.53 (m, 6H), 2.60 (q, ^3J(H,H) = 7.6 Hz, 2H), 3.37–3.48 (m, 1H), 3.54–3.64 (m, 1H), 3.75–4.00 (m, 14H), 4.08–4.13 (m, 6H), 4.29–4.32 (m, 4H), 4.63 (brs, 1H), 6.76 (s, 2H), 6.77 (s, 2H), 6.84 (d, ^3J(H,H) = 8.9 Hz, 2H), 6.94–6.97 (m, 2H), 7.09–7.15 (m, 10H), 7.30–7.44 (m, 6H), 7.80 (d, ^3J(H,H) = 8.4 Hz, 1H), 7.85 ppm (d, ^3J(H,H) = 8.4 Hz, 1H); MS(FT-MALDI): *m*/*z* (%): 1269 (10) [M^++K], 1253 (10) [M^++Na], 1230 (100) [M^+].

Compound 14: A solution of compound **13** (0.40 g, 0.32 mmol) in THF/EtOH (40 mL, 1:1 v/v) was degassed (N_2, 10 min) before TsOH·H_2O (~10 mg, cat.) was added. The yellow solution was stirred for 16 h at room temperature, whereupon it was diluted with CH_2Cl_2 (50 mL). The combined organic phase was washed with a saturated aqueous $NaHCO_3$ solution (50 mL) and H_2O (50 mL), and dried ($MgSO_4$). Concentration in vacuo gave a yellow oil, which was subjected to column chromatography (deactivated SiO_2: CH_2Cl_2/EtOAc 1:1). The yellow band (R_f = 0.4) was collected and the solvent evaporated to give compound **14** (0.21 g, 56 %) as a yellow foam. ^{1}H NMR (300 MHz, CD_3COCD_3): δ = 1.24 (t, ^3J(H,H) = 7.6 Hz, 3H), 1.33 (s, 18H), 2.64 (q, ^3J(H,H) = 7.6 Hz, 2H), 3.50–3.75 (m, 5H), 3.82–3.86 (m, 4H), 3.91–3.94 (m, 2H), 3.97–4.03 (m, 4H), 4.08–4.19 (m, 6H), 4.32–4.36 (m, 4H), 6.80 (s, 2H), 6.81 (s, 2H), 6.89 (d, ^3J(H,H) = 8.9 Hz, 2H), 6.99–7.01 (m, 2H), 7.13–7.20 (m, 10H), 7.33–7.48 (m, 6H), 7.83–7.89 ppm (m, 2H); MS(FT-MALDI): *m*/*z* (%): 1185 (5) [M^++K], 1169 (20) [M^++Na], 1146 (100) [M^+].

Compound 15: A solution of compound **14** (0.20 g, 0.17 mmol), TsCl (0.068 g, 0.35 mmol), Et_3N (0.2 mL, 0.14 g, 1.4 mmol), and DMAP (~10 mg, cat.) in anhydrous CH_2Cl_2 (50 mL) was stirred at room temper-

ature for 20 h, whereupon the solvent was removed and the yellow solid was purified by column chromatography (deactivated SiO_2: CH_2Cl_2/EtOAc 19:1). The yellow band ($R_f = 0.6$) was collected and the solvent evaporated to give compound **15** (0.22 g, 98%) as a yellow foam. ^{1}H NMR (300 MHz, CD_3COCD_3): $\delta = 1.20$ (t, $^3J(H,H) = 7.5$ Hz, 3H), 1.33 (s, 18H), 2.36 (s, 3H), 2.60 (q, $^3J(H,H) = 7.5$ Hz, 2H), 3.77–3.83 (m, 6H), 3.86–3.96 (m, 6H), 4.07–4.15 (m, 6H), 4.20–4.25 (m, 4H), 4.29–4.32 (m, 2H), 6.75 (s, 2H), 6.77 (s, 2H), 6.83 (d, $^3J(H,H) = 9.0$ Hz, 2H), 6.94–6.97 (m, 2H), 7.09–7.15 (m, 10H), 7.30–7.35 (m, 7H), 7.39 (t, $^3J(H,H) = 8.5$ Hz, 1H), 7.77–7.83 ppm (m, 4H); MS(FT-MALDI): *m/z* (%): 1300 (100) [M^+].

Compound 16: The tosylate **15** (0.22 g, 0.17 mmol) was dissolved in anhydrous Me_2CO (50 mL) and KSCN (0.49 g, 5.04 mmol) was added in one portion. The yellow reaction mixture was heated under reflux for 1 d, whereupon additional KSCN (0.49 g, 5.04 mmol) was added. The reaction mixture was heated under reflux for further 1 d before being cooled to room temperature. After removal of the solvent, the yellow residue was dissolved in CH_2Cl_2 (100 mL), washed with H_2O (2×50 mL) and dried ($MgSO_4$). Concentration in vacuo gave 0.20 g (97%) of the compound **16** as a yellow foam. ^{1}H NMR (500 MHz, CD_3COCD_3): $\delta = 1.20$ (t, $^3J(H,H) = 7.6$ Hz, 3H), 1.29 (s, 18H), 2.60 (q, $^3J(H,H) = 7.6$ Hz, 2H), 3.37 (t, $^3J(H,H) = 5.7$ Hz, 2H), 3.78–3.81 (m, 4H), 3.89 (t, $^3J(H,H) = 4.6$ Hz, 2H), 3.93–3.95 (m, 2H), 3.99 (t, $^3J(H,H) = 4.6$ Hz, 2H), 4.04–4.08 (m, 2H), 4.09–4.13 (m, 6H), 4.29–4.31 (m, 2H), 4.33–4.35 (m, 2H), 6.76 (s, 2H), 6.77 (s, 2H), 6.84 (d, $^3J(H,H) = 8.8$ Hz, 2H), 6.95–6.98 (m, 2H), 7.10–7.15 (m, 10H), 7.30–7.32 (m, 4H), 7.37 (t, $^3J(H,H) = 8.5$ Hz, 1H), 7.42 (t, $^3J(H,H) = 8.5$ Hz, 1H), 7.81 (d, $^3J(H,H) = 8.5$ Hz, 1H), 7.85 (d, $^3J(H,H) = 8.5$ Hz, 1H); IR (KBr): $\tilde{\nu} = 2154$ cm^{-1} (S–C≡N); MS(FT-MALDI): *m/z* (%): 1226 (15) [M^++K], 1210 (15) [M^++Na], 1187 (100) [M^+].

Dumbbell 1: Compound **16** (0.19 g, 0.16 mmol) and the chloride **17** (0.14 g, 0.18 mmol) were dissolved in anhydrous THF/EtOH (2:1 v/v, 50 mL), after which powdered $NaBH_4$ (0.060 g, 1.6 mmol) was added in one portion. The reaction mixture was stirred for 1 d at room temperature, whereupon additional $NaBH_4$ (0.060 g, 1.6 mmol) was added and the reaction mixture was stirred for further 3 d at room temperature. Thereafter, it was poured into an ice-cooled saturated aqueous NH_4Cl solution (50 mL) and extracted with CH_2Cl_2 (2×50 mL). The combined organic extracts were dried ($MgSO_4$) and concentration in vacuo gave a yellow oil, which was purified by column chromatography (deactivated SiO_2: CH_2Cl_2/EtOAc 3:2). The yellow band ($R_f = 0.4$) was collected and the solvent evaporated affording compound **1** (0.21 g, 68%) as a yellow foam. ^{1}H NMR (500 MHz, CD_3COCD_3): $\delta = 1.20$ (t, $^3J(H,H) = 7.6$ Hz, 3H), 1.29 (s, 18H), 2.60 (m, 4H), 3.29 (s, 9H), 3.48–3.50 (m, 6H), 3.62–3.64 (m, 6H), 3.75–3.82 (m, 14H), 3.84–3.86 (m, 2H), 3.92–3.94 (m, 4H), 4.07–4.12 (m, 12H), 4.24–4.27 (m, 2H), 4.30–4.32 (m ,2H), 4.87 (s, 2H), 4.96 (s, 4H), 6.74 (s, 2H), 6.74 (s, 2H), 6.75 (s, 2H), 6.80–6.98 (m, 10H), 7.10–7.15 (m, 10H), 7.28–7.41 (m, 12H), 7.79 (d, $^3J(H,H) = 8.6$ Hz, 1H), 7.83 ppm (d, $^3J(H,H) = 8.6$ Hz, 1H); MS(MALDI-TOF): *m/z* (%): 1925 (100) [M^+]; elemental analysis calcd (%) for $C_{110}H_{128}N_2O_{18}S_5$: C 68.58, H 6.70, N 1.45; found: C 68.41, H 6.75, N 1.29.

[2]Rotaxane RBPTTF·4PF$_6$: A solution of the dumbbell **1** (0.20 g, 0.10 mmol), **2**·2PF$_6$ (0.22 g, 0.31 mmol), and the dibromide **3** (0.082 g, 0.31 mmol) in anhydrous DMF (8 mL) was transferred to a teflon tube and subjected to 10 kbar of pressure at room temperature for 3 d. The greenish-brown solution was directly subjected to column chromatography (deactivated SiO_2) and unreacted dumbbell was eluted with Me_2CO, whereupon the eluent was changed to Me_2CO/NH_4PF_6 (1.0 g NH_4PF_6 in 100 mL Me_2CO) and the greenish brown band was collected. Most of the solvent was removed in vacuo ($T < 30$ °C), followed by addition of H_2O (100 mL). The resulting precipitate was collected by filtration, washed with H_2O (2×20 mL) and Et_2O (2×30 mL) and dried in vacuo over P_2O_5, affording compound RBPTTF·4PF$_6$ (0.15 g, 47%) as a brown solid. The data given below are for the 1:1 mixture of the two translational isomers; ^{19}F NMR (376 MHz, CD_3COCD_3): $\delta = -72.4$ ppm (d, $J = 709$ Hz); ^{31}P NMR (161 MHz, CD_3COCD_3): $\delta = -144.2$ (septet, $J = 709$ Hz); MS(ES): *m/z* (%): 1369 (15) [$M^{2+}-2PF_6$], 864 (80) [$M^{3+}-3PF_6$], 612 (100) [$M^{4+}-4PF_6$]; elemental analysis calcd (%) for $C_{146}H_{160}F_{24}N_6O_{18}P_4S_5$·2H$_2$O: C 57.25, H 5.40, N 2.74, S 5.23; found: C 57.05, H 5.20, N 2.82, S 5.04.

2-Cyanoethylthio-5-ethylthio-1,3-dithiole-2-thione (20): A solution of compound **19** (6.09 g, 20.0 mmol) in anhydrous MeCN (150 mL) was degassed (N_2, 5 min) before a solution of NaOMe (7.6 mL of a 2.75 M solution in MeOH, 20.9 mmol) was added dropwise to the yellow solution by means of a syringe over a period of 45 min at room temperature. The red mixture was stirred for 15 min, whereupon EtI (3.9 mL, 7.70 g, 49.5 mmol) was added in one portion and the reaction mixture was stirred for 24 h at room temperature. The solvent was evaporated and the resulting red oil was dissolved in CH_2Cl_2 (250 mL), washed with H_2O (3× 200 mL), and dried ($MgSO_4$). Removal of the solvent gave a red oil, which was purified by column chromatography (SiO_2: CH_2Cl_2/cyclohexane 4:1). The second yellow band ($R_f = 0.35$) was collected and concentrated, affording a yellow oil, which was repeatedly dissolved in CH_2Cl_2 (2×50 mL) and concentrated to give compound **20** (5.14 g, 92%) as a red oil, which solidified upon standing to give a yellow solid. M.p. 49.5–50.5 °C; ^{1}H NMR (300 MHz, $CDCl_3$): $\delta = 1.36$ (t, $^3J(H,H) = 7.4$ Hz, 3H), 2.74 (t, $^3J(H,H) = 7.1$ Hz, 2H), 2.95 (q, $^3J(H,H) = 7.4$ Hz, 2H), 3.08 ppm (t, $^3J(H,H) = 7.1$ Hz, 2H); ^{13}C NMR (75 MHz, $CDCl_3$): $\delta = 14.8$, 18.7, 30.8, 31.8, 117.1, 129.3, 142.4, 210.2 ppm; IR (KBr): $\tilde{\nu} = 2247$ cm^{-1} (C≡N); MS(EI): *m/z* (%): 279 (100) [M^+], 88 (84); elemental analysis calcd (%) for $C_8H_9NS_5$: C 34.38, H 3.25, N 5.01, S 57.36; found: C 34.60, H 3.22, N 5.07, S 57.48.

2-[4-(2-Cyanoethylthio)-5-ethylthio-1,3-dithiole-2-yliden]-5-tosyl-1,3-dithiolo[4,5-*c*]-pyrrole (22): Ketone **21** (1.87 g, 6.01 mmol) and thione **20** (1.68 g, 6.01 mmol) were suspended in distilled $(EtO)_3P$ (50 mL) and heated to 135 °C (during heating the two solids dissolved leaving a red solution and after 10–15 min a yellow orange precipitate was formed). Two additional portions of **20** (each containing 0.84 g, 3.01 mmol) were added after 15 and 30 min, respectively. The red reaction mixture was stirred for another 3 h at 135 °C, cooled to room temperature and addition of MeOH (150 mL) yielded a yellow solid, which was filtered and washed with MeOH (3×50 mL). The yellow solid was subjected to column chromatography (SiO_2: CH_2Cl_2) and the yellow band ($R_f = 0.4$) was collected and the solvent evaporated to give a yellow solid, which was dissolved in CH_2Cl_2/MeOH (1:1 v/v, 500 mL) and concentrated to approximately half of its volume to precipitate the product. The yellow crystals were collected by filtration, washed with MeOH (50 mL), and dried in vacuo to give compound **22** (2.40 g, 74%) as yellow needles. M.p. 200–201 °C; ^{1}H NMR (300 MHz, CD_3SOCD_3): $\delta = 1.25$ (t, $^3J(H,H) = 7.3$ Hz, 3H), 2.38 (s, 3H), 2.84 (t, $^3J(H,H) = 6.6$ Hz, 2H), 2.89 (q, $^3J(H,H) = 7.3$ Hz, 2H), 3.11 (t, $^3J(H,H) = 6.6$ Hz, 2H), 7.39 (s, 2H), 7.46 (d, $^3J(H,H) = 8.3$ Hz, 2H), 7.82 ppm (d, $^3J(H,H) = 8.3$ Hz, 2H); ^{13}C NMR (75 MHz, CD_3SOCD_3): $\delta = 15.0$, 18.1, 21.1, 29.9, 30.9, 112.3, 112.8 (2 signals), 117.8, 118.9, 124.0, 125.9, 126.0, 126.8, 129.8, 130.4, 134.4, 145.9 ppm; IR (KBr): $\tilde{\nu} = 2250$ cm^{-1} (C≡N); MS(EI): *m/z* (%): 542 (11) [M^+], 387 (28) [M^+−Ts], 184 (55), 105 (100), 91 (65); elemental analysis calcd (%) for $C_{20}H_{18}N_2O_2S_7$: C 44.25, H 3.34, N 5.16, S 41.35; found: C 44.40, H 3.34, N 5.23, S 41.42.

Compound 23: A solution of the iodide **18** (0.95 g, 1.05 mmol) and **22** (0.55 g, 1.01 mmol) in anhydrous THF (70 mL) was degassed (N_2, 10 min) before a solution of CsOH·H$_2$O (0.174 g, 1.04 mmol) in anhydrous MeOH (5.0 mL) was added dropwise by means of a syringe over a period of 75 min at room temperature. Subsequently, the reaction mixture was stirred for 2 d at room temperature, whereupon the yellow reaction mixture was diluted with CH_2Cl_2 (150 mL), washed with brine (150 mL), H_2O (2×150 mL), and dried ($MgSO_4$). Removal of the solvent gave a yellow foam, which was purified by column chromatography (SiO_2: CH_2Cl_2/cyclohexane 9:1). The broad yellow band ($R_f = 0.35$) was collected and concentrated, affording a yellow foam, which was repeatedly dissolved in CH_2Cl_2 (2×30 mL) and concentrated to give compound **23** (0.99 g, 77%) as a yellow foam. ^{1}H NMR (300 MHz, CD_3COCD_3): $\delta = 1.20$ (t, $^3J(H,H) = 7.6$ Hz, 3H), 1.23 (t, $^3J(H,H) = 7.4$ Hz, 3H), 1.29 (s, 18H), 2.38 (s, 3H), 2.61 (q, $^3J(H,H) = 7.6$ Hz, 2H), 2.84 (q, $^3J(H,H) = 7.4$ Hz, 2H), 3.10 (t, $^3J(H,H) = 6.3$ Hz, 2H), 3.84 (t, $^3J(H,H) = 6.3$ Hz, 2H), 3.93–3.99 (m, 4H), 4.02–4.06 (m, 2H), 4.14–4.19 (m, 2H), 4.27–4.33 (m, 4H), 6.84 (d, $^3J(H,H) = 9.0$ Hz, 2H), 6.89–6.97 (m, 2H), 7.06–7.14 (m,

10H), 7.24 and 7.27 (AB q, $J=2.1$ Hz, 2H), 7.28–7.43 (m, 8H), 7.80–7.85 ppm (m, 4H); MS(MALDI-TOF): *m/z* (%): 1265 (22) [M^+], 1111 (100) [M^++H−Ts]; HiRes-FT-MALDI-MS: *m/z* calcd for $C_{70}H_{75}NO_7S_7^+$: 1265.3583; found: 1265.3580; elemental analysis calcd (%) for $C_{70}H_{75}NO_7S_7$: C 66.37, H 5.97, N 1.11, S 17.72; found: C 65.88, H 5.94, N 1.30, S 17.75.

Compound 24: Compound **23** (0.85 g, 0.67 mmol) was dissolved in anhydrous THF/MeOH (1:1 v/v, 70 mL) and degassed (N_2, 10 min) before NaOMe (25% solution in MeOH, 2.3 mL, 0.54 g, 10.1 mmol) was added in one portion. The yellow solution was heated under reflux for 15 min before being cooled to room temperature, whereupon the solvent was evaporated. The yellow residue was dissolved in CH_2Cl_2 (100 mL), washed with H_2O (3×100 mL) and dried ($MgSO_4$). Concentration gave a yellow foam, which was subjected to column chromatography (SiO_2: CH_2Cl_2). The yellow band ($R_f=0.5$) was collected and concentrated to provide compound **24** (0.64 g, 87%) as a yellow foam. ^{1}H NMR (300 MHz, CD_3COCD_3): $\delta=1.21$ (t, ^3J(H,H)=7.6 Hz, 3H), 1.26 (t, ^3J(H,H)=7.3 Hz, 3H), 1.30 (s, 18H), 2.61 (q, ^3J(H,H)=7.6 Hz, 2H), 2.87 (q, ^3J(H,H)=7.3 Hz, 2H), 3.11 (t, ^3J(H,H)=6.4 Hz, 2H), 3.86 (t, ^3J(H,H)=6.4 Hz, 2H), 3.95–4.01 (m, 4H), 4.02–4.05 (m, 2H), 4.16–4.19 (m, 2H), 4.29–4.33 (m, 4H), 6.79 and 6.80 (AB q, $J=1.9$ Hz, 2H), 6.85 (d, ^3J(H,H)=9.0 Hz, 2H), 6.93 (d, ^3J(H,H)=8.0 Hz, 1H), 6.96 (d, ^3J(H,H)=8.0 Hz, 1H), 7.06–7.14 (m, 10H), 7.26–7.38 (m, 6H), 7.83 (d, ^3J(H,H)=8.0 Hz, 1H), 7.86 (d, ^3J(H,H)=8.0 Hz, 1H), 10.36 ppm (br s, 1H); MS(MALDI-TOF): *m/z* (%): 1112 (100) [M^+]; HiRes-FT-MALDI-MS: *m/z* calcd for $C_{63}H_{69}NO_5S_6^+$: 1111.3495; found: 1111.3452; elemental analysis calcd (%) for $C_{63}H_{69}NO_5S_6$: C 68.01, H 6.25, N 1.26, S 17.29; found: C 67.74, H 6.36, N 1.28, S 17.06.

Compound 26: Compounds **24** (0.61 g, 0.55 mmol) and **25** (0.25 g, 0.90 mmol) were dissolved in anhydrous DMF (20 mL) and degassed (N_2, 10 min) before NaH (0.055 g of a 60% suspension in mineral oil, 1.38 mmol) was added. The reaction mixture was stirred for 3.5 h at room temperature, causing the initially yellow solution to become more orange. Brine (80 mL) was added dropwise until no more gas evolution was observed and the resulting yellow precipitate was filtered, washed with H_2O (20 mL), and dried. The crude product was purified by column chromatography (SiO_2: CH_2Cl_2). The yellow band ($R_f=0.5$) was collected and the solvent evaporated, providing compound **26** (0.50 g, 75%) as a yellow foam. ^{1}H NMR (300 MHz, CD_3COCD_3): $\delta=1.21$ (t, ^3J(H,H)=7.6 Hz, 3H), 1.26 (t, ^3J(H,H)=7.3 Hz, 3H), 1.30 (s, 18H), 2.61 (q, ^3J(H,H)=7.6 Hz, 2H), 2.86 (q, ^3J(H,H)=7.3 Hz, 2H), 3.11 (t, ^3J(H,H)=6.4 Hz, 2H), 3.61–3.73 (m, 4H), 3.74–3.78 (m, 2H), 3.85 (t, ^3J(H,H)=6.4 Hz, 2H), 3.94–4.00 (m, 4H), 4.02–4.05 (m, 2H), 4.08–4.12 (m, 2H), 4.15–4.19 (m, 2H), 4.28–4.34 (m, 4H), 6.76 and 6.79 (AB q, $J=2.0$ Hz, 2H), 6.85 (d, ^3J(H,H)=9.0 Hz, 2H), 6.93 (d, ^3J(H,H)=8.0 Hz, 1H), 6.96 (d, ^3J(H,H)=8.0 Hz, 1H), 7.06–7.13 (m, 10H), 7.26–7.38 (m, 6H), 7.83 (d, ^3J(H,H)=8.0 Hz, 1H), 7.86 ppm (d, ^3J(H,H)=8.0 Hz, 1H); MS(MALDI-TOF): *m/z* (%): 1217 (100) [M^+]; HiRes-FT-MALDI-MS: *m/z* calcd for $C_{67}H_{76}ClNO_6S_6^+$: 1217.3680; found: 1217.3675; elemental analysis calcd (%) for $C_{67}H_{76}ClNO_6S_6$: C 66.01, H 6.28, N 1.15, S 15.78; found: C 66.14, H 6.30, N 1.20, S 15.61.

Compound 27: The chloride **26** (0.46 g, 0.38 mmol) was dissolved in anhydrous Me_2CO (60 mL) and NaI (3.42 g, 22.8 mmol) was added in one portion. The reaction mixture was heated under reflux for 6 d, before being cooled to room temperature and the solvent removed in vacuo. The yellow residue was dissolved in CH_2Cl_2 (75 mL) and washed with H_2O (3×50 mL), before being dried ($MgSO_4$). Concentration in vacuo gave compound **27** (0.49 g, 99%) as a yellow foam. ^{1}H NMR (300 MHz, CD_3COCD_3): $\delta=1.21$ (t, ^3J(H,H)=7.6 Hz, 3H), 1.26 (t, ^3J(H,H)=7.3 Hz, 3H), 1.30 (s, 18H), 2.61 (q, ^3J(H,H)=7.6 Hz, 2H), 2.86 (q, ^3J(H,H)=7.3 Hz, 2H), 3.11 (t, ^3J(H,H)=6.4 Hz, 2H), 3.30 (t, ^3J(H,H)=6.5 Hz, 2H), 3.69 (t, ^3J(H,H)=6.5 Hz, 2H), 3.74–3.78 (m, 2H), 3.85 (t, ^3J(H,H)=6.4 Hz, 2H), 3.95–4.01 (m, 4H), 4.02–4.06 (m, 2H), 4.08–4.12 (m, 2H), 4.16–4.19 (m, 2H), 4.29–4.34 (m, 4H), 6.77 and 6.80 (AB q, $J=2.1$ Hz, 2H), 6.85 (d, ^3J(H,H)=9.0 Hz, 2H), 6.93 (d, ^3J(H,H)=8.0 Hz, 1H), 6.96 (d, ^3J(H,H)=8.0 Hz, 1H), 7.06–7.14 (m, 10H), 7.26–7.38 (m, 6H), 7.83 (d, ^3J(H,H)=8.0 Hz, 1H), 7.86 ppm (d, ^3J(H,H)=8.0 Hz, 1H); MS(MALDI-TOF): *m/z* (%): 1309 (100) [M^+]; HiRes-FT-MALDI-MS: *m/z* calcd for $C_{67}H_{76}INO_6S_6^+$: 1309.3036; found: 1309.3035; elemental analysis calcd (%) for $C_{67}H_{76}INO_6S_6$: C 61.40, H 5.84, N 1.07, S 14.68; found: C 61.78, H 5.83, N 1.11, S 14.50.

Compound 28: The iodide **27** (0.48 g, 0.37 mmol) was dissolved in anhydrous Me_2CO (50 mL) and KSCN (1.78 g, 18.3 mmol) was added in one portion. The yellow reaction mixture was heated under reflux for 3 d, whereupon the reaction mixture was cooled to room temperature. After removal of the solvent, the yellow residue was dissolved in CH_2Cl_2 (100 mL), washed with H_2O (3×75 mL), and dried ($MgSO_4$). Concentration in vacuo gave compound **28** (0.45 g, 99%) as a yellow foam. ^{1}H NMR (300 MHz, CD_3COCD_3): $\delta=1.21$ (t, ^3J(H,H)=7.6 Hz, 3H), 1.26 (t, ^3J(H,H)=7.3 Hz, 3H), 1.30 (s, 18H), 2.61 (q, ^3J(H,H)=7.6 Hz, 2H), 2.87 (q, ^3J(H,H)=7.3 Hz, 2H), 3.11 (t, ^3J(H,H)=6.4 Hz, 2H), 3.28 (t, ^3J(H,H)=5.7 Hz, 2H), 3.76–3.81 (m, 4H), 3.86 (t, ^3J(H,H)=6.4 Hz, 2H), 3.94–4.01 (m, 4H), 4.03–4.06 (m, 2H), 4.11–4.14 (m, 2H), 4.16–4.19 (m, 2H), 4.29–4.34 (m, 4H), 6.77 and 6.80 (AB q, $J=2.1$ Hz, 2H), 6.85 (d, ^3J(H,H)=9.0 Hz, 2H), 6.93 (d, ^3J(H,H)=8.0 Hz, 1H), 6.96 (d, ^3J(H,H)=8.0 Hz, 1H), 7.06–7.14 (m, 10H), 7.26–7.38 (m, 6H), 7.83 (d, ^3J(H,H)=8.0 Hz, 1H), 7.86 ppm (d, ^3J(H,H)=8.0 Hz, 1H); IR (KBr): $\tilde{\nu}=2154$ cm^{-1} (S−C≡N); MS(MALDI-TOF): *m/z* (%): 1241 (100) [M^+]; HiRes-FT-MALDI-MS: *m/z* calcd for $C_{68}H_{76}N_2O_6S_7^+$: 1240.3743; found: 1240.3743; elemental analysis calcd (%) for $C_{68}H_{76}N_2O_6S_7$: C 65.77, H 6.17, N 2.26, S 18.08; found: C 65.87, H 6.31, N 2.28, S 17.83.

Dumbbell 29: The chloride **17** (0.19 g, 0.24 mmol) and compound **28** (0.25 g, 0.20 mmol) were dissolved in anhydrous THF/EtOH (2:1 v/v, 50 mL), after which powdered $NaBH_4$ (0.15 g, 3.97 mmol) was added in one portion. The reaction mixture was stirred for 2 d at room temperature, whereupon it was poured into a saturated aqueous NH_4Cl solution (50 mL), and extracted with CH_2Cl_2 (2×75 mL). The combined organic extracts were washed with brine (100 mL) and dried ($MgSO_4$). Concentration in vacuo gave a yellow oil, which was purified by column chromatography (SiO_2: CH_2Cl_2/EtOAc 2:1). The yellow band ($R_f=0.5$) was collected and the solvent evaporated affording a yellow oil, which was repeatedly dissolved in CH_2Cl_2 (2×25 mL) and concentrated to give compound **29** (0.31 g, 78%) as a yellow foam. ^{1}H NMR (300 MHz, CD_3COCD_3): $\delta=1.21$ (t, ^3J(H,H)=7.6 Hz, 3H), 1.24 (t, ^3J(H,H)=7.3 Hz, 3H), 1.30 (s, 18H), 2.52 (t, ^3J(H,H)=6.4 Hz, 2H), 2.61 (q, ^3J(H,H)=7.6 Hz, 2H), 2.84 (q, ^3J(H,H)=7.3 Hz, 2H), 3.08 (t, ^3J(H,H)=6.4 Hz, 2H), 3.29 (s, 9H), 3.49 (t, ^3J(H,H)=6.4 Hz, 2H), 3.48–3.51 (m, 6H), 3.62–3.67 (m, 10H), 3.77–3.82 (m, 6H), 3.83 (t, ^3J(H,H)=6.4 Hz, 2H), 3.93–3.98 (m, 4H), 4.01–4.18 (m, 12H), 4.26–4.32 (m, 4H), 4.91 (s, 2H), 5.03 (s, 4H), 6.73 (s, 2H), 6.76 and 6.78 (AB q, $J=2.0$ Hz, 2H), 6.82 (d, ^3J(H,H)=8.5 Hz, 2H), 6.85 (d, ^3J(H,H)=9.1 Hz, 2H), 6.92 (d, ^3J(H,H)=8.0 Hz, 1H), 6.94 (d, ^3J(H,H)=8.0 Hz, 1H), 6.95 (d, ^3J(H,H)=8.6 Hz, 4H), 7.07–7.14 (m, 10H), 7.26–7.35 (m, 8H), 7.39 (d, ^3J(H,H)=8.6 Hz, 4H), 7.83 (d, ^3J(H,H)=8.0 Hz, 1H), 7.86 ppm (d, ^3J(H,H)=8.0 Hz, 1H); MS(MALDI-TOF): *m/z* (%): 1976 (100) [M^+], 1767 (12); HiRes-FT-MALDI-MS: *m/z* calcd for $C_{110}H_{131}NO_{18}S_7^+$: 1977.7406; found: 1977.7405; elemental analysis calcd (%) for $C_{110}H_{131}NO_{18}S_7$: C 66.74, H 6.67, N 0.71, S 11.34; found: C 66.64, H 6.45, N 0.77, S 11.15.

[2]Rotaxane RBLOCK·4PF$_6$: A solution of the dumbbell **29** (0.25 g, 0.13 mmol), **2**·2PF$_6$ (0.27 g, 0.38 mmol), and the dibromide **3** (0.10 g, 0.38 mmol) in anhydrous DMF (12 mL) was transferred to a teflon-tube and subjected to 10 kbar of pressure at room temperature for 3 d. The red solution was directly subjected to column chromatography (SiO_2) and unreacted dumbbell was eluted with Me_2CO, whereupon the eluent was changed to Me_2CO/NH_4PF_6 (1.0 g NH_4PF_6 in 100 mL Me_2CO) and the red band was collected. Most of the solvent was removed in vacuo ($T<30$ °C), followed by addition of H_2O (100 mL). The resulting precipitate was collected by filtration, washed with H_2O (2×20 mL) and Et_2O (2×30 mL) and dried in vacuo over P_2O_5, affording 0.16 g (41%) of the compound RBLOCK·4PF$_6$ as a red solid. Data for RBLOCK·4PF$_6$: mp 170 °C (decomposed without melting); ^{1}H NMR (400 MHz, CD_3COCD_3): $\delta=1.18$ (t, ^3J(H,H)=7.6 Hz, 3H), 1.27 (s, 18H), 1.30 (t, ^3J(H,H)=7.3 Hz, 3H), 2.56 (t, ^3J(H,H)=6.2 Hz, 2H), 2.58 (q, ^3J(H,H)=7.6 Hz, 2H), 2.72 (d, ^3J(H,H)=8.0 Hz, 1H), 2.74 (d, ^3J(H,H)=8.0 Hz, 1H), 2.93 (q, ^3J(H,H)=7.3 Hz, 2H), 3.29 (s, 9H), 3.41–3.46 (m, 2H), 3.48–3.52 (m, 6H), 3.55 (t, ^3J(H,H)=6.5 Hz, 2H), 3.63–3.69 (m, 8H), 3.71 (s, 2H),

3.74–3.82 (m, 6H), 4.02–4.22 (m, 10H), 4.34–4.45 (m, 6H), 4.48–4.62 (m, 6H), 4.90 (s, 2H), 5.04 (s, 4H), 6.01–6.14 (br m, 8H), 6.15 (t, ^3J(H,H) = 8.0 Hz, 1H), 6.24 (t, ^3J(H,H) = 8.0 Hz, 1H), 6.44 (d, ^3J(H,H) = 8.0 Hz, 1H), 6.45 (d, ^3J(H,H) = 8.0 Hz, 1H), 6.66 and 6.72 (AB q, J = 2.2 Hz, 2H), 6.78 (s, 2H), 6.80–6.96 (m, 8H), 7.03–7.10 (m, 10H), 7.26–7.34 (m, 6H), 7.40 (d, ^3J(H,H) = 8.4 Hz, 4H), 7.50–7.90 (br m, 8H), 8.10–8.50 (br m, 8H), 9.05–9.45 ppm (br m, 8H); UV/Vis (MeCN, 298 K): λ_{max} (ε) = 540 nm (920 $mol^{-1}dm^{-3}cm^{-1}$); MS (MALDI-TOF): m/z (%): 2644 (8) [$M^+ - 3PF_6$], 2499 (8) [$M^+ - 4PF_6$], 1977 (2), 665 (16) [CBPQT+PF_6^+], 561 (100); elemental analysis calcd (%) for $C_{146}H_{163}F_{24}N_5O_{18}P_4S_7 \cdot 2H_2O$: C 56.27, H 5.40, N 2.25, S 7.20; found: C 56.23, H 5.32, N 2.46, S 7.50.

Data analysis: Exponential decay curves were obtained for each temperature by recording the CV over a range of different scan rates utilizing a modification of previously used methods.[25,55] The time interval, t, was determined as the time between formation of the MSCC—reduction to the TTF neutral redox state—and its oxidation to the monocationic state, equivalent to the point of measurement of the proportion of MSCC remaining. The proportion of MSCC remaining N_{MSCC}/N_{Total} was obtained by integrating the area under the peak of the MSCC in the second anodic scan, N_{MSCC}, and then normalized to a single electron (N_{Total}, $1e^-$) by halving the total area ($2e^-$) of the first or second anodic scan. The integrated areas were determined from normalized data. The accuracy of the normalizing procedure was checked by comparing the integrated area from each of the anodic and cathodic scans and was found to vary by no more than $\pm 5\%$. The integration regions were selected to include the contributions to the CV from the diffusional tail that follows the main peak. Two additional points were added to the decay curve that correspond to time zero, $t = 0$ s, $N_{MSCC}/N_{Total} = 1.0$ and, at long relaxation times, $t = 300$ s, at which the value of N_{MSCC}/N_{Total} was set equal to the steady-state value determined by the first anodic scan. The resulting decay curve was fitted to a single exponential curve in order to obtain the time constant, τ, and hence the rate constant, k at T. Errors in the kinetics data (τ, k, and $\Delta G^{\ddagger}$) were obtained from the absolute errors determined from the fit of each decay curve (N_{MSCC}/N_{Total} versus t). Errors in the $\Delta H^{\ddagger}$ and $\Delta S^{\ddagger}$ parameters were obtained from the errors in the fits to the Eyring plots. Errors in the equilibrium thermodynamics data were estimated from the van't Hoff plots.

Derivation of the kinetic parameters: The kinetic data—rate constants and activation barriers—for the relaxation from the MSCC back to the equilibrium ratio of MSCC:GSCC were acquired based on the following equilibrium [Eq. (3)]:

$$\mathrm{MSCC} \underset{k_2}{\overset{k_1}{\rightleftharpoons}} \mathrm{GSCC} \tag{3}$$

The relative concentration of the MSCC as a function of time can be denoted as $x_t = [\mathrm{MSCC}]/[\mathrm{Total}]$, where t is the time. Let $x_0 = x_{t=0}$, and at equilibrium, let $x_{eq} = x_{t\to\infty}$. The first derivative of $x(t)$ with respect to time is given by Equation (4).

$$\begin{aligned} &\mathrm{d}[\mathrm{MSCC}]/\mathrm{d}t = -k_1 x[\mathrm{Total}] + k_2(1-x)[\mathrm{Total}] \\ &\Rightarrow \mathrm{d}x/\mathrm{d}t = -k_1 x + k_2(1-x) \end{aligned} \tag{4}$$

Integration of Equation (4) leads to the following equality [Eq. (5)]

$$\begin{aligned} &\int_{x_0}^{x_t} \frac{\mathrm{d}x}{(k_1+k_2)x - k_2} = \int_0^t -(k_1+k_2)\mathrm{d}t \\ &\Rightarrow \ln\frac{(k_1+k_2)x_t - k_2}{(k_1+k_2)x_0 - k_2} = -(k_1+k_2)t \end{aligned} \tag{5}$$

At equilibrium, $0 = \mathrm{d}x/\mathrm{d}t = -k_1 x + k_2(1-x) \Rightarrow k_2 = (k_1 x_{eq})/(1-x_{eq})$. Putting this expression for k_2 into Equation (5), we obtain Equation (6).

$$x_t = x_{eq} + (x_0 - x_{eq})\exp[-k_1 t/(1-x_{eq})] = a + b\exp(-t/\tau) \tag{6}$$

By substituting the relationship $k_1 = (1-x_{eq})/\tau$ into the expression $\Delta G^{\ddagger} = -RT\ln(hk_1/k_B T)$, $\Delta G^{\ddagger}$ can be calculated.

For the MSTJ devices, x_{eq} cannot be obtained on account of the fact that N_{MSCC}/N_{Total} cannot be measured directly. As a result, the kinetic data for the MSTJ were acquired based on the assumption that the current associated with the pure GSCC (I_{GSCC}) is much smaller than the current associated with the pure switch-closed state (I_{CLOSED}). Given this assumption, the following approximate equality holds $N_{MSCC}/N_{Total} \approx I_{OPEN}/I_{CLOSED}$, as elaborated in the next section. The assumption $I_{GSCC} \ll I_{CLOSED}$ has been verified by the theoretical studies.[36]

Derivation of switching amplitudes in MSTJ devices: Based on the refined hypothesis that, the high-conductance (switch-closed) state of an MSTJ corresponds to the MSCC, but that the low-conductance (switch-open) state is related to the MSCC/GSCC ratio at equilibrium, the measured current (I) can be defined in terms of the intrinsic conductance properties of each co-conformation and the percentage of the co-conformations N_{MSCC}/N_{Total} and N_{GSCC}/N_{Total}.

Consequently, I_{OPEN} corresponds to a thermal equilibrium condition and is a mixture of the GSCC and MSCC, whereas I_{CLOSED} is 100% of the MSCC. This model influences the meaning of the ratio I_{OPEN}/I_{CLOSED}.

The conductance properties of these systems can be described as follows: Firstly, the GSCC and MSCC have intrinsic current values I_{GSCC} and I_{MSCC}, which are constants at a certain temperature T. Therefore, at any time the current measured (I_t) is a summation of these two contributions. The magnitude of each contribution is scaled by the proportions of the GSCC (N_{GSCC}/N_{Total}) and MSCC (N_{MSCC}/N_{Total}) present in the mixture. This leads to the following general formula [Eq. (7)] for the current I_t:

$$I_t = (N_{MSCC}/N_{Total})_t I_{MSCC} + (N_{GSCC}/N_{Total})_t I_{GSCC} \tag{7}$$

Therefore, for the trivial situation when I_{CLOSED} is measured at $t = 0$, we assume that $N_{GSCC} = 0$ and $N_{MSCC}/N_{Total} = 1$ confirming that $I_{CLOSED} = I_{MSCC}$ (see Figure 9).

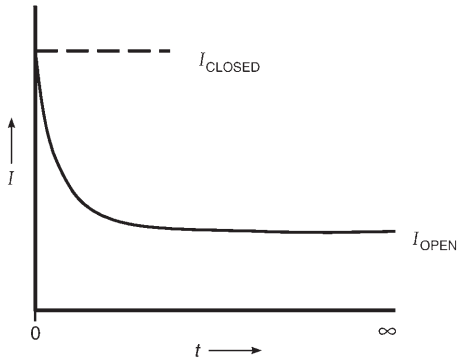

Figure 9. Schematic representation of a volatility curve defining I_{CLOSED} and I_{OPEN}.

Now consider what happens at thermal equilibrium ($t = \infty$), defined as I_{OPEN} [Eq. (8)]

$$I_{OPEN} = (N_{MSCC}/N_{Total})_\infty I_{CLOSED} + (N_{GSCC}/N_{Total})_\infty I_{GSCC} \tag{8}$$

Consequently, the ratio I_{OPEN}/I_{CLOSED}, which happens to be the inverse of the switching amplitude, can be expressed as Equation (9).

$$I_{OPEN}/I_{CLOSED} = (N_{MSCC}/N_{Total})_\infty + (N_{GSCC}/N_{Total})_\infty (I_{GSCC}/I_{CLOSED}) \tag{9}$$

If the intrinsic conductance of the GSCC is very small compared to I_{CLOSED}, the term I_{GSCC}/I_{CLOSED} goes to zero and therefore we can use Equation (10).

$$I_{OPEN}/I_{CLOSED} = N_{MSCC}/N_{Total} \tag{10}$$

For example, in the case of R(A)TTF^{4+}, $N_{MSCC}/N_{Total}=1/10$ and assuming an intrinsic conductance of the GSCC that is 100 times smaller than the MSCC, $I_{GSCC}/I_{Closed}=1/100$ then the ratio at $t=\infty$ is given by Equation (11)

$$I_{OPEN}/I_{CLOSED} = 1/10 + (9/10 \times 1/100) = 1/10 + 9/1000 = 0.1 + 0.009 = 0.109 \quad (11)$$

Consider also how RBPTTF^{4+} behaves at low temperatures (MSCC/GSCC=3:4) [Eq. (12)]

$$I_{OPEN}/I_{CLOSED} = 3/7 + (4/7 \times 1/100) = 0.43 + 0.006 = 0.436 \quad (12)$$

In other words, the ratio of N_{MSCC}/N_{Total} dominates the I_{OPEN}/I_{CLOSED} measured ratio at equilibrium and therefore the switching amplitude in the condition when the intrinsic conductance of the GSCC is small.

Whereas in the condition when the intrinsic conductance of the GSCC were higher such as if $I_{GSCC}/I_{CLOSED}=1/10$, then for R(A)TTF^{4+} and RBPTTF^{4+} Equations (13) and (14), respectively, are valid.

$$I_{OPEN}/I_{CLOSED} = 1/10 + (9/10 \times 1/10) = 1/10 + 9/100 = 0.1 + 0.09 = 0.19 \quad (13)$$

$$I_{OPEN}/I_{CLOSED} = 3/7 + (4/7 \times 1/10) = 0.43 + 0.06 = 0.49 \quad (14)$$

Comparison between the two cases, in which I_{GSCC} is comparatively smaller (1%) or larger (10%), leads to switching amplitudes for R(A)TTF^{4+} of 9 and 5, respectively, whereas for RBPTTF^{4+} they correspond to 2.3 and 2.0.

Small intrinsic conductances of the GSCC relative to the MSCC are not so unlikely and have been calculated[36] for related TTF-containing bistable catenanes, based on the theory of coherent electron transport, to be approximately 1/10000.

Acknowledgements

This research was funded by the Office of Naval Research (ONR), the National Science Foundation (NSF), the Molectronics Program of the Defense Advanced Research Project Agency (DARPA), the Microelectronics Advance Research Corporation (MARCO) and its Focus Center on Functional Engineered NanoArchitectonics (FENA) and Materials, Structures and Devices, and the Center for Nanoscale Innovation for Defense (CNID) in the US and by the Danish Natural Science Research Council (SNF, grants #21-03-0014 and #21-03-0317), the Oticon and MODECS foundation in Denmark. J.W.C. acknowledges the Samsung Lee Kun Hee Scholarship Foundation for a graduate fellowship. N.N.P.M. acknowledges The Netherlands Organization for Scientific Research (NWO) for a TALENT fellowship.

[1] R. L. McCreery, *Chem. Mater.* **2004**, *16*, 4477–4496.
[2] A. Nitzan, *Annu. Rev. Phys. Chem.* **2001**, *52*, 681–750.
[3] J. R. Heath, M. A. Ratner, *Phys. Today* **2003**, *56*, 43–49.
[4] H. McConnell, *J. Chem. Phys.* **1961**, *35*, 508–515.
[5] a) P. S. Vincett, G. G. Robert, *Thin Solid Films* **1980**, *68*, 135–171; b) K. V. Mikkelsen, M. A. Ratner, *Chem. Rev.* **1987**, *87*, 113–153.
[6] a) E. E. Polymeropoulos, J. Sagiv, *J. Chem. Phys.* **1978**, *69*, 1836–1847; b) T. Lee, W. Wang, J. F. Klemic, J. J. Zhang, J. Su, M. A. Reed, *J. Phys. Chem. B* **2004**, *108*, 8742–8750.
[7] a) D. L. Allara, T. D. Dunbar, P. S. Weiss, L. A. Bumm, M. T. Cygan, J. M. Tour, W. A. Reinerth, Y. Yao, M. Kozaki, L. Jones, *Ann. N. Y. Acad. Sci.* **1998**, *852*, 349–370; b) J. Chen, M. A. Reed, A. M. Rawlett, J. M. Tour, *Science* **1999**, *286*, 1550–1552; c) T. D. Dunbar, M. T. Cygan, L. A. Bumm, G. S. McCarty, T. P. Burgin, W. A. Reinerth, L. Jones, J. J. Jackiw, J. M. Tour, P. S. Weiss, D. L. Allara, *J. Phys. Chem. B* **2000**, *104*, 4880–4893; d) Z. J. Donhauser, B. A. Mantooth, K. F. Kelly, L. A. Bumm, J. D. Monnell, J. J. Stapleton, D. W. Price, A. M. Rawlett, D. L. Allara, J. M. Tour, P. S. Weiss, *Science* **2001**, *292*, 2303–2307.
[8] J. F. Smalley, S. B. Sachs, C. E. Chidsey, S. P. Dudek, H. D. Sikes, S. E. Creager, C. J. Yu, S. W. Feldberg, M. D. Newton, *J. Am. Chem. Soc.* **2004**, *126*, 14620–14630.
[9] a) P. E. Kornilovitch, A. M. Bratkovsky, R. S. Williams, *Phys. Rev. B* **2002**, *66*, 165436, 1–11; b) Y. Chen, G. Y. Jung, D. A. Ohlberg, M. Li, D. R. Stewart, J. O. Jeppesen, K. A. Nielsen, J. F. Stoddart, R. S. Williams, *Nanotechnology* **2003**, *14*, 462–468; c) C. A. Richter, D. R. Stewart, D. A. Ohlberg, R. S. Williams, *Appl. Phys. A* **2005**, *80*, 1355–1362.
[10] a) A. Aviram, M. A. Ratner, *Chem. Phys. Lett.* **1974**, *29*, 277–283; b) J. Jortner, M. Ratner, *Molecular Electronics*, Blackwell Science, Oxford, **1997**.
[11] R. L. Carroll, C. B. Gorman, *Angew. Chem.* **2002**, *114*, 4556–4579; *Angew. Chem. Int. Ed.* **2002**, *41*, 4378–4400.
[12] G. Maruccio, R. Cingolani, R. Rinaldi, *J. Mater. Chem.* **2004**, *14*, 542–554.
[13] G. Ho, J. R. Heath, M. Kondratenko, D. Perepichka, K. Arseneault, M. Pezolet, M. Bryce, *Chem. Eur. J.* **2005**, *11*, 2914–2922.
[14] a) G. J. Ashwell, J. R. Sambles, A. S. Martin, W. G. Parker, *J. Chem. Soc. Chem. Commun.* **1990**, 1374–1376; b) A. S. Martin, J. R. Sambles, G. J. Ashwell, *Phys. Rev. Lett.* **1993**, *70*, 218–221; c) G. J. Ashwell, D. S. Gandolfo, *J. Mater. Chem.* **2001**, *11*, 246–248; d) G. J. Ashwell, D. S. Gandolfo, *J. Mater. Chem.* **2002**, *12*, 411–415; e) G. J. Ashwell, D. S. Gandolfo, R. Hamilton, *J. Mater. Chem.* **2002**, *12*, 416–420; f) G. J. Ashwell, W. D. Tyrrell, A. J. Whittam, *J. Am. Chem. Soc.* **2004**, *126*, 7102–7110.
[15] a) R. M. Metzger, B. Chen, U. Höpfner, M. V. Lakshmikantham, D. Vuillaume, T. Kawai, X. L. Wu, H. Tachibana, T. V. Hughes, H. Sakurai, J. W. Baldwin, C. Hosch, M. P. Cava, L. Brehmer, G. J. Ashwell, *J. Am. Chem. Soc.* **1997**, *119*, 10455–10466; b) R. M. Metzger, *Acc. Chem. Res.* **1999**, *32*, 950–957; c) T. Xu, I. R. Peterson, M. V. Lakshmikantham, R. M. Metzger, *Angew. Chem.* **2001**, *113*, 1799–1802; *Angew. Chem. Int. Ed.* **2001**, *40*, 1749–1752; d) R. M. Metzger, T. Xu, I. R. Peterson, *J. Phys. Chem. B* **2001**, *105*, 7280–7290; e) R. M. Metzger, *Chem. Rev.* **2003**, *103*, 3803–3834.
[16] a) M.-K. Ng, L. Yu, *Angew. Chem.* **2002**, *114*, 3750–3753; *Angew. Chem. Int. Ed.* **2002**, *41*, 3598–3601; b) P. Yiang, G. M. Morales, W. You, L. Yu, *Angew. Chem.* **2004**, *116*, 4571–4575; *Angew. Chem. Int. Ed.* **2004**, *43*, 4471–4475.
[17] F. C. Krebs, H. Spanggaard, N. Rozlosnik, N. B. Larsen, M. Jørgensen, *Langmuir* **2003**, *19*, 7873–7880.
[18] a) S. C. Chang, Z. Y. Li, C. N. Lau, B. Larade, R. S. Williams, *Appl. Phys. Lett.* **2003**, *83*, 3198–3200; b) D. R. Stewart, D. A. Ohlberg, P. A. Beck, Y. Chen, R. S. Williams, J. O. Jeppesen, K. A. Nielsen, J. F. Stoddart, *Nano Lett.* **2004**, *4*, 133–136; c) N. Lau, D. R. Stewart, R. S. Williams, M. Bockrath, *Nano Lett.* **2004**, *4*, 569–572.
[19] A. N. Shipway, I. Willner, *Acc. Chem. Res.* **2001**, *34*, 421–432.
[20] C. P. Collier, G. Mattersteig, E. W. Wong, Y. Luo, K. Beverly, J. Sampaio, F. M. Raymo, J. F. Stoddart, J. R. Heath, *Science* **2000**, *289*, 1172–1175.
[21] C. P. Collier, J. O. Jeppesen, Y. Luo, J. Perkins, E. W. Wong, J. R. Heath, J. F. Stoddart, *J. Am. Chem. Soc.* **2001**, *123*, 12632–12641.
[22] Y. Luo, C. P. Collier, J. O. Jeppesen, K. A. Nielsen, E. DeIonno, G. Ho, J. Perkins, H.-R. Tseng, T. Yamamoto, J. F. Stoddart, J. R. Heath, *ChemPhysChem* **2002**, *3*, 519–525.
[23] H. Yu, Y. Luo, K. Beverly, J. F. Stoddart, H.-R. Tseng, J. R. Heath, *Angew. Chem.* **2003**, *115*, 5884–5889; *Angew. Chem. Int. Ed.* **2003**, *42*, 5706–5711.
[24] M. R. Diehl, D. W. Steuerman, H.-R. Tseng, S. A. Vignon, A. Star, P. C. Celestre, J. F. Stoddart, J. R. Heath, *ChemPhysChem* **2003**, *4*, 1335–1339.
[25] D. W. Steuerman, H.-R. Tseng, A. J. Peters, A. H. Flood, J. O. Jeppesen, K. A. Nielsen, J. F. Stoddart, J. R. Heath, *Angew. Chem.* **2004**, *116*, 6648–6653; *Angew. Chem. Int. Ed.* **2004**, *43*, 6486–6491.
[26] H.-R. Tseng, D. Wu, N. X. Fang, X. Zhang, J. F. Stoddart, *ChemPhysChem* **2004**, *5*, 111–116.

[27] A. H. Flood, A. J. Peters, S. A. Vignon, D. W. Steuerman, H.-R. Tseng, S. Kang, J. R. Heath, J. F. Stoddart, *Chem. Eur. J.* **2004**, *10*, 6558–6564.

[28] a) J. O. Jeppesen, J. Perkins, J. Becher, J. F. Stoddart, *Org. Lett.* **2000**, *2*, 2631–2634; b) J. O. Jeppesen, J. Perkins, J. Becher, J. F. Stoddart, *Angew. Chem.* **2001**, *113*, 1256–1261; *Angew. Chem. Int. Ed.* **2001**, *40*, 1216–1221; c) J. O. Jeppesen, K. A. Nielsen, J. Perkins, S. A. Vignon, A. DiFabio, R. Ballardini, M. T. Gandolfi, M. Venturi, V. Balzani, J. Becher, J. F. Stoddart, *Chem. Eur. J.* **2003**, *9*, 2982–3007; d) T. Yamamoto, H. R. Tseng, J. F. Stoddart, V. Balzani, A. Credi, F. Marchioni, M. Venturi, *Collect. Czech. Chem. Commun.* **2003**, *68*, 1488–1514; e) H.-R. Tseng, S. A. Vignon, P. C. Celestre, J. Perkins, J. O. Jeppesen, A. DiFabio, R. Ballardini, M. T. Gandolfi, M. Venturi, V. Balzani, J. F. Stoddart, *Chem. Eur. J.* **2004**, *10*, 155–172; f) S. Kang, S. A. Vignon, H.-R. Tseng, J. F. Stoddart, *Chem. Eur. J.* **2004**, *10*, 2555–2564; g) I. C. Lee, C. W. Frank, T. Yamamoto, H.-R. Tseng, A. H. Flood, J. F. Stoddart, J. O. Jeppesen, *Langmuir* **2004**, *20*, 5809–5828; h) J. O. Jeppesen, S. Nygaard, S. A. Vignon, J. F. Stoddart, *Eur. J. Org. Chem.* **2005**, 196–220.

[29] a) E. Katz, O. Lioubashevsky, I. Willner, *J. Am. Chem. Soc.* **2004**, *126*, 15520–15532; b) D. Ryan, S. N. Rao, H. Rensmo, D. Fitzmaurice, J. A. Preece, S. Wenger, J. F. Stoddart, N. Zaccheroni, *J. Am. Chem. Soc.* **2000**, *122*, 6252–6257; c) B, Long, K. Nikitin, D. Fitzmaurice, *J. Am. Chem. Soc.* **2003**, *125*, 15490–15498.

[30] a) A. M. Brouwer, C. Frochot, F. G. Gatti, D. A. Leigh, L. Mottier, F. Paolucci, S. Roffia, G. W. H. Wurpel, *Science* **2001**, *291*, 2124–2128; b) A. Altieri, G. Bottari, F. Dehez, D. A. Leigh, J. K. Y. Wong, F. Zerbetto, *Angew. Chem.* **2003**, *115*, 2398–2402; *Angew. Chem. Int. Ed.* **2003**, *42*, 2296–2300; c) A. Alteri, F. G. Gatti, E. R. Kay, D. A. Leigh, D. Martel, F. Paolucci, A. M. Z. Slawin, J. K. Y. Wong, *J. Am. Chem. Soc.* **2003**, *125*, 8644–8654; d) F. Cecchet, P. Rudolf, S. Rapino, M. Margotti, F. Paolucci, J. Baggerman, A. M. Brouwer, E. R. Kay, J. K. Y. Wong, D. A. Leigh, *J. Phys. Chem. B* **2004**, *108*, 15192–15199.

[31] a) A. Livoreil, C. O. Dietrich-Buchecker, J. P. Sauvage, *J. Am. Chem. Soc.* **1994**, *116*, 9399–9400; b) J. P. Collin, P. Gavina, J. P. Sauvage, *New J. Chem.* **1997**, *21*, 525–528; c) L. Raehm, J. M. Kern, J. P. Sauvage, *Chem. Eur. J.* **1999**, *5*, 3310–3317; d) I. Poleschak, J. M. Kern, J. P. Sauvage, *Chem. Commun.* **2004**, 474–476.

[32] Although the Coulombic driven switching movement of the $CBPQT^{4+}$ ring has not been measured, we estimate that the barrier corresponding to the mono- and dication $TTF^{2+/+}$ would be at least ~3 and ~6 kcal mol^{-1}, respectively, less than the 16 kcal mol^{-1} barrier observed for the free-energy barrier between the MSCC and GSCC leading to room temperature time constants of t~500 and 3 ms, respectively.

[33] K. Nørgaard, J. O. Jeppesen, B. W. Laursen, J. B. Simonsen, M. J. Weygand, K. Kjaer, J. F. Stoddart, T. Bjørnholm, *J. Phys. Chem. B* **2005**, *109*, 1063–1066.

[34] B. W. Laursen, S. Nygaard, J. O. Jeppesen, J. F. Stoddart, *Org. Lett.* **2004**, *6*, 4167–4170.

[35] A. H. Flood, J. F. Stoddart, D. W. Steuerman, J. R. Heath, *Science* **2004**, *306*, 2055–2056.

[36] a) W. Deng, R. P. Muller, W. A. Goddard III, *J. Am. Chem. Soc.* **2004**, *126*, 13562–13563; b) Y. Kim, S. Jang, Y. Jang, W. A. Goddard III, *Phys. Rev. Lett.* **2005**, *94*, 156801, 1–4.

[37] a) K. N. Houk, S. Menzer, S. P. Newton, F. M. Raymo, J. F. Stoddart, D. J. Williams, *J. Am. Chem. Soc.* **1999**, *121*, 1479–1487; b) F. M. Raymo, M. D. Bartberger, K. N. Houk, J. F. Stoddart, *J. Am. Chem. Soc.* **2001**, *123*, 9264–9267.

[38] M. J. Blandamer, P. M. Cullis, J. B. F. N. Engberts, *J. Chem. Soc. Faraday Trans.* **1998**, *94*, 2261–2267.

[39] a) P. R. Ashton, R. Ballardini, V. Balzani, S. E. Boyd, A. Credi, M. T. Gandolfi, M. GomezLopez, S. Iqbal, D. Philp, J. A. Preece, L. Prodi, H. G. Ricketts, J. F. Stoddart, M. S. Tolley, M. Venturi, A. J. P. White, D. J. Williams, *Chem. Eur. J.* **1997**, *3*, 152–170; b) P. R. Ashton, V. Balzani, J. Becher, A. Credi, M. C. T. Fyfe, G. Mattersteig, S. Menzer, M. B. Nielsen, F. M. Raymo, J. F. Stoddart, M. Venturi, D. J. Williams, *J. Am. Chem. Soc.* **1999**, *121*, 3951–3957.

[40] M. B. Nielsen, J. O. Jeppesen, J. Lau, C. Lomholt, D. Damgaard, J. Jacomsen, J. Becher, J. F. Stoddart, *J. Org. Chem.* **2001**, *66*, 3559–3563.

[41] R. Castro, K. R. Nixon, J. D. Evanseck, A. Kaifer, *J. Org. Chem.* **1996**, *61*, 7298–7303.

[42] The impact of temperature on equilibrium constants, K and their associated population ratios, MSCC/GSCC, are related by the van't Hoff equation $[\ln(K_1/K_2) = -(\Delta H/R)(1/T_1 - 1/T_2)]$ such that it is the enthalpic contribution that determines the temperature sensitivity in K.

[43] J. O. Jeppesen, K. Takimiya, F. Jensen, T. Brimert, K. Nielsen, N. Thorup, J. Becher *J. Org. Chem.* **2000**, *65*, 5794–5805.

[44] J. G. Hansen, K. S. Bang, N. Thorup, J. Becher, *Eur. J. Org. Chem.* **2000**, 2135–2144.

[45] P.-L. Anelli, P. R. Ashton, R. Ballardini, V. Balzani, M. T. Gandolfi, T. T. Goodnow, A. E. Kaifer, D. Philp, M. Pietraszkiewicz, L. Prodi, M. V. Reddington, A. M. Z. Slawin, N. Spencer, C. Vicent, D. J. Williams, *J. Am. Chem. Soc.* **1992**, *114*, 193–218.

[46] N. Svenstrup, K. M. Rasmussen, T. K. Hansen, J. Becher, *Synthesis* **1994**, 809–812.

[47] C. L. Butler, A. G. Renfrew, L. H. Cretcher, B. L. Souther, *J. Am. Chem. Soc.* **1937**, *59*, 227–229.

[48] D. D. Perrin, W. L. F. Armarego, *Purification of Laboratory Chemicals*, Pergamon, New York, **1988**.

[49] $\Delta G^{\neq}$ at each temperature was calculated from the Eyring equation: $\Delta G^{\neq} = -RT\ln(hk/k_BT)$ in which R, h, k and k_B are the gas constant, Planck's constant, the first-order rate constant and Boltzmann constant, respectively. k corresponds to $(1-x_{eq})/\tau$, in which x_{eq} is N_{MSCC}/N_{Total} at equilibrium and τ is 1/e decay time constant. $\Delta H^{\neq}$ and $\Delta S^{\neq}$ were obtained from the regression analysis of Gibbs–Helmholtz plot, $\Delta G^{\neq}/T$ vs $1/T$.

[50] The activation barrier (E_a) was calculated from the Arrhenius equation: $k = A\exp(-E_a/RT)$ in which A is the activation coefficient. E_a was obtained from a regression analysis of the Arrhenius plots, $\ln k$ vs $1/T$.

[51] The remnant molecular signature is a sequence of voltage pulses of 1 s that are applied to poly-Si electrodes with 100 mV step sizes and, in between each pulse, is a read voltage of +0.1 V held for 1.5 s to record the current. The metal top electrodes were connected to ground through a preamplifier.

[52] V. Daniel, *Dielectric Relaxation*, Academic Press, **1967**.

[53] M. Iwamoto, C. Wu, *Phys. Rev. E* **1997**, *56*, 3721–3724.

[54] To the first order, the normalized current at equilibrium defined by the I_{OPEN}/I_{CLOSED} ratio is approximately equal to N_{MSCC}/N_{Total} if the intrinsic conductance of the GSCC is smaller than the MSCC by more than two orders of magnitude.

[55] a) R. S. Nicholson, I. Shain, *Anal. Chem.* **1964**, *36*, 706–723; b) L. Raehm, J.-M. Kern, J.-P. Sauvage, *Chem. Eur. J.* **1999**, *5*, 3310–3317.

Received: August 1, 2005
Published online: December 1, 2005

